2010

Late Permian Paleoenvironmental Factors Expounded Through Analysis of a Forest-Floor Paleosol Profile, Karoo Basin, South Africa

Cassi Knight
Colby College

LATE PERMIAN PALEOENVIRONMENTAL FACTORS EXPOUNDED THROUGH ANALYSIS OF A FOREST-FLOOR PALEOSOL PROFILE, KAROO BASIN, SOUTH AFRICA

Except where reference is made to the work of others, the work described in this thesis is my own or was done in collaboration with my advisory committee

Cassi Knight ‘10

Certificate of Approval:

Dr. Robert A. Gastaldo, Chairman
Whipple Coddington Professor
Department of Geology

Dr. Valerie Reynolds
Claire Boothe Luce Assistant Professor
Department of Geology

Dr. Bruce F. Rueger
Visiting Assistant Professor
Department of Geology

LATE PERMIAN PALEOENVIRONMENTAL FACTORS EXPOUNDED THROUGH ANALYSIS OF A FOREST-FLOOR PALEOSOL PROFILE, KAROO BASIN, SOUTH AFRICA

Cassi Knight ‘10

A Thesis

Submitted to the Faculty of the Geology Department of
Colby College in Fulfillment of the Requirements for
Honors in Geology

Waterville, Maine

May, 2010

Abstract

Beaufort Group paleosols from the Karoo Basin, South Africa, record the paleoenvironmental conditions that existed prior to and after the Permian-Triassic extinction event. Paleosol exposures from Wapadsberg Pass, Eastern Cape Province, represent a well-preserved forest-floor litter overlying an interpreted inceptisol, a condition unique to the basin. Vegetation that colonized this landscape included a canopy of the gymnosperm *Glossopteris* and an understory of sphenopsids (*Phyllotheca* and *Trizygia*). Wapadsberg Pass paleosol sites were sampled for petrographic and geochemical analyses to constrain interpretations of Late Permian paleoenvironmental conditions that existed ~ 70 m below the Permian-Triassic Boundary (PTB). This project focuses on determining paleosol-nutrient quality to test a hypothesis that plant toxicity may be responsible for the reported decrease in *Glossopteris*-leaf size prior to the PTB event.

The greenish-grey (5GY 6/1) paleosol is an iron-stained siltstone with intervals of bedded very-fine sand to silt. The paleosol has a maximum thickness of 70 cm, with a coarser interval at ~30 cm depth. The litter horizon is concentrated in the upper 20 cm of the profile, and includes remnants of poorly preserved *Glossopteris* leaves and *Vertebraria* roots. Rooting structures penetrate to ~70 cm depth. Tuffite is interspersed in and caps the paleosol.

Primary structures in petrographic section include ripples, parallel bedding, and small-scale soft-sediment deformation. These are partially destroyed due to phytoturbation and bioturbation. All paleosol sites examined contain an identifiable tuffite, characterized as a mix of well-rounded to angular, transparent clasts. These are distributed as irregular pockets cross-cutting bedding and as dispersed isolated clasts within the fine matrix. Analytical results from TOC and TOC:TON obtained using elemental analysis, and geochemical data obtained using ICP-OES and XRF instruments.

High resolution stratigraphic and geochemical investigation of this paleosol reveals that it is an inceptisol, formed on an aggradational floodplain colonized by a *Glossopteris* forest, and contains elevated concentrations of plant-toxic elements.

Acknowledgements

Many thanks to Dr. Robert Gastaldo for providing the opportunity to travel to South Africa to complete the fieldwork necessary for this project, and for all his time and effort spent being an excellent advisor. His guidance and knowledge throughout this project were indispensable. Thanks to an extremely knowledgeable and helpful field research team, who taught me so much and made South Africa unforgettable. Thanks also to Dr. Valerie Reynolds for all her time and patience assisting with ICP-OES analysis and to Ellen Crapster-Pregont for many hours spent in the lab. Thanks to Dr. Bruce Rueger for his help with clay slide preparation. Thanks to Dr. Don Allen, who helped even though he didn't have to. Thank you to Dr. David Gibson at UMF for graciously allowing the use of his XRF, and to Dr. Neil Tabor for all his suggestions and knowledge regarding paleosols. This project would not have been possible without generous funding from the Sullivan-Garner Fund grant and Claire Boothe Luce funding from the Dean of Faculty at Colby College.

Table of Contents

Introduction

The Permian-Triassic mass extinction event, at ~252.6 Ma (Mundil et al., 2004) is well documented in the marine realm, and is estimated to have killed off over 90% of marine taxa, as well as up to 82% of terrestrial vertebrate taxa (Ward et al., 2005). However, the terrestrial record of this extinction event is not as definitive as that preserved in marine deposits. The Karoo Basin, South Africa, is hailed as containing the most complete and continuous sedimentological record of the Permian and Triassic (Ward et al., 2005; Prevec et al., in press), and exposing rocks contemporaneous to those recording the Permian-Triassic boundary (PTB) in the marine realm. Hence, the Karoo strata are interpreted to contain evidence for the terrestrial response to the marine Permian-Triassic extinction event (Ward et al., 2000, 2005; Retallack et al., 2003; Gastaldo et al., 2009). In an attempt to correlate the terrestrial PTB with the marine event, many stratigraphic, biostratigraphic, stable isotopic, paleomagnetic, and whole-rock geochemical studies have focused on the Karoo Basin (Smith, 1995; Smith and Ward, 2001, Retallack et al., 2003; DeKock and Kirschvink, 2004; Ward et al., 2005; Smith and Botha, 2005; Botha and Smith, 2006; Gastaldo et al., 2005, 2009; Reid et al., 2006, 2007; Tabor et al., 2007; Coney et al., 2007; Prevec et al, in press). The terrestrial PTB currently is defined by vertebrate biostratigraphy, and is placed at the last appearance datum (LAD) of *Dicynodon* (Ward et al., 2005). This horizon is found at the contact between the Permian Elandsberg member and the Triassic Palingkloof member (subunits of the Balfour formation, Adelaide subgroup, Beaufort Group, Karoo Supergroup). Variation in climate is interpreted to be one mechanism that induced the continental extinction, and a shift from seasonally wet to more seasonally arid conditions is reported across the PTB based on a change in fluvial style from meandering to braided rivers (Ward et al., 2000; Smith and Ward, 2001) at the same horizon.

This investigation uses geochemical analytical methods on a Late Permian (Elandsberg Member) paleosol, outcropping at Wapadsberg Pass in an attempt to constrain the paleoclimatic conditions present leading up to the PTB. While this study may not help to constrain the current placement of the PTB at Wapadsberg Pass, it may clarify some interpretations of environmental conditions prior to the boundary event.

Karoo Supergroup

The Karoo Supergroup, South Africa, spans approximately 110 Ma from the Late Carboniferous through the Early Jurassic. The sediments in this 12-km thick succession accumulated in an asymmetrical retro-foreland basin, which resulted from the assembly of Pangea (Catuneau et al., 1998). The tectonic activity was in response to the subduction of the paleo-Pacific plate beneath the Gondwanan plate, triggering basinal subsidence and building the adjacent Cape Fold Belt that served as the provenance for basin sediments (Smith et al., 1993). Sedimentation began following the retreat of glaciers that covered the Karoo during the Carboniferous-Middle Permian, and started filling the basin with glacial deposits in a deep-water environment (Catuneau et al., 1998). After deglaciation, the basin began to shallow and sedimentation continued as fluvial-lacustrine and eolian deposits (Catuneau et al., 1998).

General Stratigraphy

The sediments filling the Karoo Basin are assigned to the Karoo Supergroup, and the rocks purported to contain the PTB occur several 1000 m above its base. The succession begins with the Carboniferous Dwyka Group, which records the deglaciation of Gondwana, and ends in the Jurassic with the Clarens-Elliot Groups. The Karoo Supergroup is divided into the Dwyka Group, Ecca Group, Beaufort Group, and the Molteno and Clarens-Elliot formations (Fig. 1). The rocks that transition across the Permian-Triassic boundary occur within the Beaufort Group, which is considered to be the first fully continental sequence in the supergroup.

Dwyka Group- The Dwyka Group is a glacially derived succession composed of diamictite, shale, and sandstone deposited during a Late Paleozoic episode of deglaciation that covered Gondwana. The diamictites are thinly bedded to massive, and contain matrix-supported clasts of pebble to cobble-sized rocks. The clasts display a wide range of compositions and rock-types that include vein quartz, quartzite, banded ironstone, dolomite, slate, granite, gneiss, and amygdaloidal lava in an argillaceous and arenaceous matrix (Smith et al., 1993). The upper contact of the Dwyka Group is with the Ecca Group, and marks the beginning of the Permian at 290 Ma. The Ecca represents the final deglaciation of Gondwana.

Ecca Group- The Ecca Group consists of deep-water and coastal sediments that were deposited in a closed interior water body. The lower Ecca group is made up of inter-bedded mudstone and sandstone that represent turbidite deposits accumulated within a shallow inland sea (Ecca Sea). The Ecca Sea was fed by glacial meltwater, and its southern margin began to prograde northeast following the deglaciation of Gondwana (Johnson et al., 2006). Progradation occurred as large deltas built out across the coastline, resulting in thick deposits that overlie the Dwyka turbidite sequences. This transgression also is reflected by the distribution of the turbidites, which show deposition in increasingly shallow environments over time (Johnson et al., 2006). Deltaic and coastal plain deposition eventually filled enough of the basin to end an Ecca Sea, and the dominant depositional setting became broad alluvial flood plains.

Beaufort Group- The Beaufort Group is the first fully continental sequence in the Karoo Supergroup, and is divided into the Adelaide subgroup (further separated into the Koonap, Middleton, and Balfour formations) and the overlying Tarkastad subgroup (separated into the Katberg and Burgersdorp formations) (Johnson et al., 2006) (Fig. 1). The Beaufort Group consists of alluvial plain deposits, which are aggradational floodplain and fluvial sediments beginning in the middle Permian and extending to the early Triassic. Sediments of the Beaufort Group are mostly red-and-purple sandstone that fines upwards into red-and-purple mudstone, and includes abundant vertebrate fossils, desiccation cracks, and paleopedogenic carbonate-nodule horizons (Smith et al., 1993). These features, considered to be characteristic of Beaufort Group members, indicate that aggradational floodplain deposits dominate this succession.

In the Eastern Cape Province, the lower Beaufort (equivalent to the Adelaide subgroup) is characterized by thinly laminated lacustrine mudstone, rippled siltstone, and thin discontinuous lenses of sandstone. The Adelaide subgroup rocks are interpreted to be fluvio-lacustrine sediments deposited under a humid climate that allowed for the establishment of wet floodplains with high water tables (Smith et al., 1993). The upper Adelaide subgroup (upper Balfour Fm.), however, exhibits a change in fluvial style, and deposits consist of thick (>10 m) meandering channel-sandstone bodies. Above this, the upper Beaufort Group (equivalent to the Tarkastad subgroup) begins at the first occurrence of intraformational mud pebbles, pedogenic carbonate

clasts, and sand-filled mud cracks, which mark the base of the Katberg formation (Smith and Ward, 2001; Smith and Botha, 2005; Botha and Smith, 2006; Johnson et al., 2006). The upper Beaufort Group is a sequence of mixed silt-and-sandstone fluvial deposits with stacked tabular sandstone bodies, interpreted to be the result of braided river deposition under a more arid climate. The Katberg formation (upper Beaufort Group) is mostly composed of sandstone that has been characterized as arenaceous (Smith et al., 1993), while the overlying Molteno formation (upper Beaufort Group) is characterized as argillaceous (Johnson et al., 2006).

The Balfour Formation

The Balfour formation is the uppermost unit in the Adelaide subgroup, and consists of the Oudeberg, Daggaboersnek, Barberkrans, Elandsberg, and Palingkloof members. The Permian-Triassic boundary (PTB) is placed between the uppermost two members, reported to reside at the contact between the greenish grey siltstone of the Permian Elandsberg Member and the overlying reddish grey siltstones of the Triassic Palingkloof Member (Ward et al., 2000; Retallack et al., 2003) (Fig. 1). Ward et al. (2000) reported that the Adelaide Subgroup undergoes a facies change across the PTB reflecting a difference in the environment of deposition, interpreted to be the result of climate change associated with the extinction event. The stratigraphic relationships and channel geometries of sandstone bodies below and above the boundary indicate the presence of large meandering channels in the Permian, and braided channels confined to the Katberg Sandstone in the Triassic (Ward et al., 2005; Pace et al., 2009).

Based on changes in stable-isotope geochemistry across the boundary (MacLeod et al., 2000), Ward et al. (2000) proposed that the latest Permian was characterized by a trend of widespread drying. If this indeed is the case, the soil-types that formed across the Karoo landscape and supported the pre-and-post extinction event vegetation should contain evidence of this change in climate. Examining soil profiles in stratigraphic section close to the recognized PTB, such as the paleosol at Wapadsberg Pass, may help to constrain climatic conditions prior to the PTB and resolve uncertainty surrounding Late-Permian trends.

Previous PTB Studies

There are only a limited number of Karoo Basin localities where rocks that span the PTB can be studied. Currently, these include Caledon and Bethulie in the Free State in the eastern Karoo (Smith, 1995; MacLeod et al., 2000; Ward et al., 2000; Smith and Ward, 2001; Botha and Smith, 2005; Smith and Botha, 2006), Carleton Heights in the Northern Cape Province, and Commando Drift (Komandodrifdam) (Ward et al. 2005), Lootsberg Pass, and Wapadsberg Pass in the Eastern Cape Province (MacLeod et al, 2000; Ward et al., 2000; Smith and Ward, 2001; Ward et al., 2005; Botha and Smith, 2005; Smith and Botha, 2006). The placement of the PTB has relied on studies of regional stratigraphic correlation and vertebrate biostratigraphy, supplemented with carbon-isotope geochemical analyses, paleomagnetic data, and whole rock geochemical studies. In previous Permian-Triassic studies (Ward et al., 2000; Ward et al., 2005; DeKock and Kirschvink, 2004; Botha and Smith, 2005; Smith and Botha, 2006), Wapadsberg Pass has played a prominent role.

Vertebrate Biostratigraphy- The most widely accepted placement of the PTB is defined by vertebrate biostratigraphy and was interpreted to reside at the base of the laminite 'event bed' (Ward et al., 2000), which sits just above the last appearance datum (LAD) of *Dicynodon* (Smith, 1995; Smith & Ward, 2001). The initial placement of the boundary at this level was based on the stratigraphic presence of an 'event bed', reported to be a dead zone void of any evidence of life (Ward et al., 2000). This placement was supplemented by Smith and Ward (2001) with biostratigraphic data reported from Bethulie and Lootsberg Pass (Smith, 1995; Ward et al, 2000). They placed the PTB at the base of the laminite bed, below which the LAD of *Dicynodon* was noted to occur in a horizon of large brown-weathering calcareous nodules, and above which is the first appearance datum (FAD) of *Lystrosaurus* (Triassic indicator taxon) (Ward et al., 2005).

Carbon-Isotope Geochemistry- MacLeod et al. (2000) reported on the stratigraphy of boundary exposures, and stable carbon-and-oxygen isotope values from calcareous soil nodules, diagenetic calcite, and *Dicynodon*, *Lystrosaurus*, and *Diictodon* tusks that were found both below and above the vertebrate defined PTB. Samples were collected at Bethulie where they straddle the PTB, and at Lootsberg Pass and Doornplaats where samples came only from the Permian. They reported a small negative $\delta^{13}C$ excursion of ~3.5‰ within a ~15 m zone of stratigraphic

overlap between Permian (*Dicynodon*) and Triassic (*Lystrosaurus*) taxa from Bethulie, and correlated this to the observed negative spike at the PTB in the marine record (MacLeod et al., 2000).

Ward et al. (2000), like Macleod et al. (2000), combined stratigraphy and stable carbon isotopic data from Wapadsberg Pass to place the PTB and the disappearance of the *Glossopteris* flora at the base of a reported 'laminite bed' in the Wapadsberg section. The base of the laminite or 'event bed' resides at the first red siltstone of the Palingkloof member where it contacts the green siltstone of the Elandsberg member, and overlies the LAD of *Dicynodon* (Ward et al., 2000). The lower contact of the laminite bed coincides with a -2‰ excursion in $\delta^{13}C$ and was reported to mark a noticeable shift in river deposit geometries across the boundary. Sandstone-body geometries below the boundary resemble deep channel-fills and are interpreted as meandering river deposits, while sandstone bodies above the boundary are more tabular and are interpreted as braided river deposits (Smith, 1995). This change in fluvial style was attributed to increased sediment load resulting from the whole scale die-off of Karoo Basin vegetation (Ward et al., 2000), however, lower total organic carbon (TOC) values are reported for the early Triassic siltstones (Gastaldo and Rolerson, 2008). The negative excursion in $\delta^{13}C$ also was attributed to the vegetational die-off, as a result of increased organic carbon input and loss of primary productivity across the boundary (Ward et al., 2000).

Subsequently, Ward et al. (2005) analyzed carbon isotopic data from pedogenic carbonate nodules in boundary sections across the Karoo, for comparison with the marine carbon isotopic pattern which showed a large negative excursion in $\delta^{13}C$ of -10‰ at the PTB. From the pedogenic nodule data Ward et al. (2005) report a drop in terrestrial $\delta^{13}C$ of -2‰ at the boundary at all localities, except Wapadsberg Pass, and they correlated this isotopic trend to a singular excursion at the PTB in the marine $\delta^{13}C$ record from the Carbonate Platform of China (Ward et al., 2005). The $\delta^{13}C$ record from Wapadsberg Pass shows no substantially negative excursions and no significant drop in $\delta^{13}C$ at the PTB, and Ward et al. (2005) attribute this indistinct pattern to homogenization of primary $\delta^{13}C$ by local igneous activity.

Paleomagnetic Studies- The remnant paleomagnetic signature retained in the rocks across the PTB was documented by DeKock and Kirschvink (2004), with the aim of constraining the correlation of the terrestrial boundary with the marine record in China. Although a magnetostratigraphy was developed for the Karoo, DeKock and Kirschvink (2004) were unable to obtain reliable data from rocks at Wapadsberg Pass due to their remagnetization by numerous intrusive dolerite dikes. Based on data from other Karoo sites, the PTB was placed to coincide with two different horizons. The first horizon reported is at a horizon of carbonate nodules immediately below the 'laminite bed', referred to as the end-Permian paleosol (EPP) and that marks the LAD of *Dicynodon* (DeKock and Kirschvink, 2004). Subsequently, the boundary was moved to the contact between the red siltstone of the Permian Elandsberg member and the green siltstone of the Triassic Palingkloof member (DeKock and Kirschvink, 2004; Ward et al., 2005). However, these two horizons are not stratigraphically isochronous, and thus are reported to occur during two different paleomagnetic intervals. The first assigned horizon occurs at the switch from R1 to N2 polarity where the 'end-Permian paleosol' and the LAD of *Dicynodon* coincide, above the first red siltstone (DeKock and Kirschvink, 2004, fig. 2), whereas the subsequent placement occurs just before the switch from an R1 interval to an N2 interval at the first red siltstone in the interval of R1 polarity (DeKock and Kirschvink, 2004, fig. 5).

Ward et al. (2005) amended the magnetostratigraphic interpretations of DeKock and Kirschvink (2004) and moved the PTB to an interval of N1 polarity occurring just above the switch from the R1 polarity. This placement corresponds to the LAD of *Dicynodon* and conforms to the succession in Meishan, China. The magnetostratigraphic correlations used to place the boundary in the Karoo Basin include the section exposed at Old Wapadsberg Pass, even though there are no paleomagnetic data from that locality (Ward et al., 2005).

The paleomagnetic data from the Karoo Basin are ambiguous and do not allow for the definitive placement of the PTB at a coeval interval of polarity. There is no agreement between authors on the type of interval, reverse or normal polarity, present during the latest Permian and earliest Triassic. DeKock and Kirschvink (2004) reported a switch from R1 to N2 polarity interval across the boundary, while Ward et al. (2005) report this as a switch from R1 to N1. The authors

do agree, however, that the extinction pattern was gradual leading up to the boundary rather than a single catastrophic event (Ward et al., 2005; DeKock and Kirshvink, 2004).

Previous Whole Rock Geochemical Studies- Few geochemical studies (Scheffler et al., 2003, 2006; Coney et al., 2007) have been undertaken in the Karoo Basin, to date. These have been used to interpret basin-wide paleoenvironmental conditions leading up to, and across the boundary event.

Scheffler et al. (2003) found that climatic variation occurred during the deposition of the Dwyka and Ecca Groups in the Carboniferous and Early-Middle Permian. Their interpretations were based on several proxies including Zr/Ti for provenance change, chemical index of alteration minus K (CIA-K) for degree of molecular weathering, Rb/K for degree of marine influence, V/Cr and $\delta^{13}C$ as measures of anoxia, and C/N as an organic matter biomarker. They observed that the glacial deposits of the Dwyka were interrupted by sedimentary units with proxy signatures suggesting a more temperate climate and less marine influence, and found that this fluctuation in climate was controlled by cyclic periods (~5 My) of glaciation and deglaciation. Periods of glaciation are represented by regressive successions in the stratigraphic record, reflected by an increase in $\delta^{13}C$ and the Rb/K ratio, and a decrease in V/Cr (Scheffler et al., 2003). During these low-stands, sedimentation occurred under non-marine conditions. Periods of deglaciation are marked by transgressions and fully marine deposition, with the development of anoxic bottom conditions during the two most pronounced instances of sea-level rise (Scheffler et al., 2003). Fully marine conditions are interpreted to have persisted into the post-glacial deposits of the Ecca Group (Scheffler et al., 2003).

Scheffler et al. (2006) interpret a climatic shift from warm and humid in the early Permian, to a warm and arid climate by the Middle Permian, again, based on the stratigraphic trends of the CIA, Zr/Ti, Rb/K, and V/Cr ratios, and total organic carbon (TOC) values. Each of these relationships has been used as a proxy for climatic conditions. Warm, arid conditions persisted into the Late Permian and are interpreted to have allowed for the spread across the basin of the *Glossopteris* flora, which is a wetland flora not known to have colonized arid environments (Coney et al., 2007). Despite this application of chemical proxies to infer paleoclimatic trends

during the Middle and Late Permian, no clear proxy signatures or trends were noted across the PTB (Scheffler et al., 2006).

Coney et al. (2007) examined the stratigraphy of Karoo P-Tr boundary sections, and reported that no marked petrographic (lithological or sedimentary) change exists across the PTB as defined by vertebrate biostratigraphy. They also noted that there is no distinct geochemical trend observed across the PTB at all localities examined (including Wapadsberg Pass). These sites exhibit wide fluctuations in sedimentary geochemistry relative to other locations in the basin, with no observable trends in their variation. Coney et al. (2007) found that the Wapadsberg Pass samples show a small increase in all siderophile and chalcophile elements across the PTB, and a marked decrease in lithophile elements (Sc, Cs, and Th) at calcareous nodule-bearing horizons. However, these changes are restricted to these horizons, do not correlate well with any other locality studied, and were not large enough to be considered significant (Coney et al., 2007). They report no changes in the abundances of rare-earth elements (REE) and that the most significant basin-wide elemental change is exhibited by iron (Fe_2O_3), which becomes more abundant above the PTB. However, this increased concentration is due to a shift in oxidation state, from Fe^{2+} to Fe^{3+}, the result of sediment exposure to atmospheric conditions (as climate became increasingly arid during the Late Permian) or from more recent post-diagenetic alteration by Fe-rich fluids (Coney et al., 2007). They concluded that Karoo geochemistry exhibits no distinctive signature across the PTB, and that variations in elemental abundance are attributed largely to changes in lithology rather than changes in climate (Coney et al., 2007). However, these conclusions are contradictory as the change in climate responsible for an increase in observed iron (Fe_2O_3) across the boundary would produce a significant geochemical signature.

South African Permian Paleosols

A clear, comprehensive description of paleosols in the Karoo Basin has yet to be developed. Paleosols were described by Smith (1995), Retallack et al. (2003), Smith and Botha (2005), and Botha and Smith (2006), but there is no agreement between the soil descriptions amongst the authors, nor is a single soil classification scheme adopted. Hence, there currently is

no classification scheme developed for Permian and Triassic (or any age) paleosols that includes distinguishing features, allowing for field identification of each soil type.

Smith (1995) briefly described paleosols in the *Dicynodon* and *Lystrosaurus* Assemblage Zones, which reside below and above the PTB, respectively. Smith (1995) described three types of Permain *Dicynodon* Zone paleosols and attributed them to different parts of the Permian landscape. Immature, entisol-type paleosols are interpreted to have formed on channel banks and levees, and preserve horizons of vertical rooting and rhizoconcretions in addition to small (<10 cm diameter) isolated calcareous nodules. More mature paleosols formed on proximal floodplains and are characterized as containing a maroon clay-enriched horizon, slickensides, and coalesced calcareous nodules with smooth tops. The most common paleosol type is a hydromorphic gleysol, formed in floodbasins bordering standing bodies of water interpreted to be ponds and lakes. These are characterized by extensive mottling (maroon or purple and greenish grey) along root traces, and contain gypsum rosettes and septarian nodules. The presence of gypsum rosettes (sulfur sourced from volcanogenic deosits) indicates the precipitation of this mineral in a warm climate, and the 'gley-type' mottles suggest periodic drying of a typically saturated solum. Smith (1995) described only one paleosol-type in the Triassic *Lystrosaurus* Zone. This soil is rubified, mottled green only around rhizoconcretions, exhibits desiccation cracks, and has greater numbers of well developed calcitic horizons containing calcareous nodules. The nodules weather dark-brown, are larger (>15 cm diameter) than those found in *Dicynodon* Zone paleosols, and sometimes coalesce into clumps. The morphology of the nodules and the desiccation cracks are similar to modern calcretes, and suggest that this soil type underwent repeated wetting and drying of the solum. This change from wet to dry paleosols across the PTB is purported to have been relatively rapid and isochronous throughout the basin (Smith, 1995).

Retallack et al. (2003) identified and defined a suite of Karoo paleosol types in the Late Permian and Early Triassic that range from immature, poorly developed to mature, well developed soils. Poorly developed Late Permian soils include the Bada, Hom, Som, and Zam types, all of which are interpreted as inceptisols. However, Bada and Som types also are referred

to as calcisols, whereas Bada and Hom types are termed protosols (Retallack et al., 2003, pg. 1141), despite the large difference between these soil types. Inceptisols are defined by an absence of distinct soil horizons, as these are too young to have developed a chemical weathering profile that results in distinct layers (USDA soil taxonomy). There are no accumulations of clay, Al, or Fe in the soil profile. Calcisols, at the other end of the spectrum, contain a horizon at which calcitic minerals have precipitated under evaporate conditions. Hence, the same soil by definition cannot be interchangeably termed an inceptisol and a calcisol. Protosols, like inceptisols, are characterized by a weak development of horizons and mineral alteration. Protosol, however, is a very broad term that refers to features and characteristics included in inceptisols and entisols. The use of terms and colors as soil-descriptors for this suite is unhelpful in classifying the Karoo Permian paleosols (Appendix 1, Pludow, A., personal communication, 2009).

Bada paleosols are characterized as grey siltstone with a few, shallow calcareous nodules and rhizoconcretions (Retallack et al., 2003, table 1). They are interpreted to have formed in floodplain depressions, under semi-arid climates that experienced a long dry season. Dry bushland vegetation is thought to have colonized these soil types. However, Bada paleosols also are characterized as gleyed floodplain soils composed of blue-grey silt with large calcareous nodules and deep root traces. This paleosol type is designated as both an inceptisol requiring 10ka for formation and as a calcisol taking 8-15ka to form (Retallack et al., 2003, table 1). These two descriptions of the same paleosol type (Bada) are contradictory.

Som paleosols are characterized by a grey siltstone surface overlying purple siltstone in which shallow calcareous nodules formed (Retallack et al., 2003, table 1). They are interpreted to have developed under semi-arid climates in floodplains covered by seasonally wet vegetation. Som paleosols also are described as red/purple calcisols with large calcareous nodules, comparable to Bada paleosols, but with more relict bedding. These defining characters, the relict bedding, and the size of the calcareous nodules are omitted from the table in which paleosol types are compared (Retallack et al., 2003, table 1), leaving it difficult to constrain this soil's characters.

Hom paleosols are described as a white to grey sandstone substrate with a few, shallow calcareous nodules and rhizoconcretions (Retallack et al., 2003, table 1). They formed under unknown climatic conditions, and are restricted to sandy levees thought to have been colonized by riparian bushland vegetation. This soil type is reported to resemble Bada paleosols with more relict bedding, deeper rooting, and calcareous nodules. Hom paleosols appear to be indistinguishable from Bada paleosols because the only difference is the presence of deeper rooting in the former (Retallack et al., 2003).

The climate in which Zam paleosols developed also is unknown, but these soil types are interpreted as having formed around lake-margins that were colonized by early successional quillworts (lycopsids). Zam paleosols are described as consisting of a purple-grey, bedded siltstone with rooting and burrow traces (Retallack et al., 2003, table 1), and also as an oxidized protosol with rooting and clear relict bedding (Retallack et al., 2003, pg.1141).

Smith and Botha (2005) and Botha and Smith (2006) describe a single type of Permian paleosol, using a different classification scheme than that developed by Retallack et al. (2003). Paleosols below the PTB are characterized as a grey to olive-grey mudstone with large brown-weathering calcareous nodules, claystone-lined root channels, and *Planolites* and *Taenidium* burrowing structures. Soil formation is interpreted to have occurred on alluvial plains and lowland floodplains (Smith and Botha, 2005; Botha and Smith, 2006). The laminite interval that was reported to occur immediately following the vertebrate-defined PTB contains little evidence for pedogenesis (Smith & Botha, 2005; Botha & Smith, 2006). These soils are poorly developed in siltstone in which *Macanopsis* burrowing and hollow aquatic isoetalean roots are reported (Retallack et al. 2003). Recently, Gastaldo & Rolerson (2008) demonstrated that the ichnotaxon *Macanopsis* is a fully marine burrow, not found in the fully terrestrial Karoo Basin. They assigned these biogenic structures to the new continental ichnogenus *Katbergia* found in the latest Permian and earliest Triassic at Carleton Heights and elsewhere.

Paleosols at Wapadsberg Pass

A sequence of stacked paleosols exposed below the vertebrate defined PTB was identified by Reid et al. (2006, 2007) in New and Old Wapadsberg Passes. They identified the

paleosol intervals using the presence of vertically to sub-vertically oriented roots or rhizoconcretions and/or horizons of calcite-cemented nodules (Reid et al., 2007). Rhizoconcretions were found to cap channel-fill sequences of siltstone, and the calcareous nodule horizons were restricted to siltstone at the top of fining-upwards overbank deposits. All paleosols were interpreted as inceptisol and gleysol intervals (Reid et al., 2006).

To date, fossil-plant assemblages have been considered scarce in this part of the basin, although several have been reported (Gastaldo et al., 2005). Reid et al. (2006, 2007) found and collected a well preserved fossil-plant assemblage, interpreted as a forest-floor litter, above one of these poorly developed paleosols in the New Wapadsberg Pass sequence. This paleosol lies stratigraphically ~70 m below the vertebrate-defined PTB exposed at Old Wapadsberg Pass (Fig. 1).

Prevec et al. (in press) describe the *in situ* fossil-flora assemblage preserved in a white claystone bed at New Wapadsberg Pass (NWP), which they interpret to represent the soil's original O-horizon. All plants in this assemblage are preserved as impressions, and identified systematically (Prevec et al., in press). They represent a low-diversity assemblage that includes the gymnosperm tree *Glossopteris*, and a *Sphenopsid*-dominated understory and groundcover of *Phyllotheca* and *Trizygia*, respectively (Fig. 2). Subjacent soil horizons preserve vertically oriented *Vertebraria* rooting structures and poorly preserved axial and leaf parts at depth.

The features exhibited by the paleosol at New Wapadsberg Pass do not correspond well with any immature Permian-age paleosols characterized by Retallack et al. (2003). The descriptions offered by Retallack et al. (2003) are based largely on paleosol color, with few other features included that would distinguish the paleosol. The soil exposed at NWP is an olive-green (5GY 6/1) siltstone overlain by a thin (13 cm) layer of fossiliferous white claystone. Below the white claystone layer, the paleosol appears relatively homogeneous in the field, with the exception of rounded clay clasts, up to 25 cm in diameter, that occur at ~30-50 cm depth within the soil profile (Fig. 3). The closest Karoo paleosol, as defined by Retallack et al. (2003), to that at NWP is the Bada-type solely because of its grey color. No poorly developed Permian paleosols are described to be olive-green in color or to include rooting specified as *Vertebraria*

('deep rooting' implies *Vertebraria*), like the Wapadsberg Pass paleosol. The paleosol at NWP conforms most closely to Smith's (1995) entisol-type paleosols with preserved vertical rooting and calcareous nodules within the soil profile (Smith, 1995). However, the NWP paleosol is unique to the Karoo in that it incorporates a white claystone layer and visible rounded clasts within its profile. Hence, the Wapadsberg Pass paleosol warrants further investigation.

The present study allows for the opportunity to assess the only complete soil profile identified, to date, proximal to the PTB in the Karoo Basin. The goals of this project are to characterize this paleosol using representative and diagnostic soil features, and describe its geochemical signature in profile. Geochemical data, petrographic thin section, and clay mineralogic analyses will provide a more comprehensive array of criteria that can be used to interpret the environment in which the paleosol formed and better constrain environmental conditions leading up to the PTB.

Materials and Methods

Wapadsberg Pass Locality

Wapadsberg Pass is located in the Eastern Cape Province, South Africa, and exposes the vertebrate defined PTB at the contact between the Elandsberg and Palingkloof members (Ward et al., 2000, 2005; Retallack et al., 2003; Prevec et al., in press). Two closely spaced areas in the region expose the Permian Elandsberg member. One area occurs in a roadcut along the R61 highway, and the second occurs adjacent to the old, now abandoned, Wapadsberg Pass Road (Fig. 4). Here, the exposures are restricted to erosional gullies, or dongas. For this study, these areas will be referred to as New Wapadsberg Pass (NWP) and Old Wapadsberg Pass (OWP), respectively.

A single paleosol horizon was found in the exposures at NWP and OWP. In New Wapadsberg Pass, this horizon crops out in the road cut along R61 (NWP: S 31° 55.927', E 24° 52.872'), and was sampled. Old Wapadsberg Pass exposes the same paleosol horizon in two separate dongas, and each profile was sampled (OWP1: S 31° 55.199', E 24° 53.666', and

OWP2: S 31° 55.108', E 24° 53.692'). The sample localities in NWP and OWP are <1 km from each other.

Regional correlation- Regional correlation between New and Old Wapadsberg Pass was accomplished in the field by tracing a prominent sandstone bed between the two localities (Reid et al., 2007). In the OWP section, this paleosol horizon and associated fossil-flora assemblage occurs ~70 m below the PTB as defined by vertebrate biostratigraphy studies in Old Wapadsberg Pass (Ward et al., 2000; 2005).

Field Methods

Stratigraphy- Stratigraphic sections were measured for the present study in the roadcut exposure along R61 in NWP and in the donga at OWP using a Jacob's staff with site level. For both sections, bed contacts were marked at lithologic changes based on sediment grain-size. All contacts were designated as sharp, lenticular, or gradational, and lithologies were described by grain-size and Munsell Color. Primary and secondary structures, fining upwards sequences, and accessory features were identified in the field and recorded.

The R61 roadcut at New Wapadsberg Pass also was photographed to construct a photomosaic in which large-scale stratigraphic and lithologic features above and below the paleosol could be identified (Fig. 5). In total, 8.8 m of section were measured and photographed, with the paleosol positioned at the approximate middle of this sequence, 5.6 m above the base.

From field measurements and lithofacies descriptions, rough stratigraphic sections were constructed for each locality at the cm-scale. These were then refined at Colby College, yielding high resolution sections for NWP and OWP. The features of the paleosol first recognized by Reid et al. (2006, 2007) are visually represented in detail in the NWP stratigraphic column.

Sampling Protocol- At the NWP and two OWP sections, hand samples were collected from (1) the white claystone overlying the fossil-plant horizon, (2) the preserved leaf litter, and (3) at 10 cm-intervals below the O-horizon to 70 cm depth. Sampling protocol involved clearing the outer few cm of rock from the vertical profile, and removing samples from the freshly exposed surface to ensure that the rock had undergone minimum weathering (Fig. 6). Several horizons were found to be iron-stained, and rocks at each sampling interval with the fewest iron stains

were preferentially sampled to avoid excess contamination by precipitated secondary mineralization. All samples were returned to Colby College for analysis. Once there, small rock chips of each sample, for all depths, were tested for carbonate using dilute HCl.

Laboratory Methods

Petrographic Thin Sections- Thin sections were made professionally (Applied Petrographics) for samples chosen to represent each different lithology within the soil profile. These were examined under a Leica DFC 290 Macroscope equipped with a Leica Z6 APO lens and image analysis software, and under an Olympus BX41 petrographic microscope. Digital images were acquired and examined to characterize the sedimentary fabric including microstratigraphic structures and other diagenetic features. Petrographic mineral identification was not conducted to determine sediment composition.

XRD Analysis- Samples from New Wapadsberg Pass, beginning at a depth of -10 cm and extending to a depth of -60 cm in the paleosol profile, were chosen for clay mineral analysis using XRD. Rock chips with the least amount of iron staining were powdered in a ceramic mortar and pestle, and then sieved at 125 μm to separate out the clay fraction. Each sample residuum was adhered using a filter-membrane peel technique (Pollastro, 1982) to four different glass slides that were treated separately in preparation for analysis. One was left untreated, one was glycolated for 24 hours to expand clay structures, and two were heated in a muffle furnace. One sample was processed at 350˚C for 1 hr. to dehydrate the sample and the other at 550˚C for 1 hr. to collapse the clay structures. Slides were analyzed using a Rigatu D-Max B two-axis X-ray diffractometer and Jade MDI 7 software for clay mineralogy.

TOC and TON- Several micrograms of each powdered sample were analyzed using a Perkins-Elmer 2400 CHNO/S instrument. Values for total organic carbon (TOC) and total organic nitrogen (TON) were acquired. Triplicate samples were burned in the elemental analyzer and averaged. Acetanilide standards (C=71.09, H=6.71, N=10.36, O=11.84) were run every 5 samples, as unknowns, to ensure data integrity and reproducibility. The resulting values for each

sample were plotted v. sample depth, with 5% error bars, to yield profiles for TOC, TON, and TOC:TON.

ICP-OES Analysis- A small amount of powdered sample (25 mg) underwent a digestion procedure for analysis by a Spectro Arcos ICP-OES instrument to acquire geochemical data. Prior to digestion, powders were ashed in a muffle furnace at 550˚C for 3 hours to burn off all organic matter. Sample preparation then followed standard HF digestion procedure (Appendix 2) (Thomas Scheck, U. of Maryland), with the additional step of heating samples in aqua-regia following treatment with HF. Control blanks and USGS Icelandic Basalt BIR-1 standards (Gladney and Roelandts, 1988) also were digested using the same procedure. These, in addition to a 71 Element Standard were run on the ICP-OES to ensure the accuracy and reproducibility of results. Major and trace-element data were collected. The ppm values for Ba and Sr were used to calculate the Ba/Sr ratio, which was plotted against paleosol profile depth for all three sample locations.

XRF Analysis- Powders were fused into a glass slides and analyzed using a Bruker AXS S4 Pioneer XRF in the Department of Geology, University of Maine- Farmington. Major element oxide (wt%) and trace element data (ppm) were collected. During preparation, several grams of each sample were heated in a muffle furnace at 350˚C for one hour to drive off any excess water. Glass disks were made of 0.5 g of dried, powdered sample and 5.5 g of x-ray flux (lithium metaborate + metraborate) mixed in platinum-gold crucibles. The crucibles were placed in a Phoenix furnace (fully automated) where this mixture was fused. Crucibles were cleaned in hot 10% HCl for 10 minutes, and rinsed with water between samples. Visualization of geochemical trends within the soil profile were carried out by Jack Moriarty and Mary Fletcher (Colby College) and show relative element abundance and ratio magnitude.

Soil Molecular Weathering Ratios- The XRF element-oxide data were used to calculate soil molecular weathering ratios, including base loss ((Ca,Mg,Na,K)/Ti), clayeyness (Al/Si), calcification ((Ca+Mg)/Al), salinization ((K+Na)/Al), mineralogical maturity (Si/Al), and mineral assemblage stability (Fe/ K) (Scheffler et al, 2003; 2006; Sheldon and Tabor, 2009). Elemental oxides were converted from wt% to molar abundance (wt%/(g element oxide/mol)) , and the

molar values were used to calculate these ratios. A template spreadsheet provided by Neil Tabor (SMU) was used to make these conversions, and ratios were plotted v. sample depth, with 5% error bars, to yield a paleosol profile.

CIA-K- Standard soil indices (chemical index of alteration: CIA-K) were calculated using XRF element-oxide data for each NWP sample to allow for further comparison with modern soil types. Element oxide abundances based on XRF analysis for Al_2O_3, CaO, Na_2O, and K_2O were converted from wt% to molar abundance using the template provided by Neil Tabor (SMU), and the molar values of each were used to calculate CAI-K values with the equation: CAI-K = $Al(Al_2O_3+CaO+Na_2O)*100$ (Sheldon et al., 2002; template provided by Neil Tabor). CAI-K values were plotted v. paleosol depth to create a profile showing the degree of weathering (element loss) within the paleosol.

Results

Lithofacies

The lithologies in the NWP and OWP stratigraphic sections (Fig. 3 and Fig. 7, respectively) range from siltstone to very fine sandstone, and are colored shades of olive-green (5Y 4/1), grayish olive (10Y 4/2), and greenish-grey (5GY 6/1). No free carbonate was found either in the paleosol or cementing the claystone balls found at -30 cm profile depth. The plant-fossil assemblage and subjacent paleosol are in a sequence of fluvial and interfluvial deposits of sandstone and siltstone (Prevec et al., in press). There is a difference in depositional style below and above the paleosol at New Wapadsberg Pass (Fig 3).

Coarse Siltstone Facies- Coarse siltstone is greenish grey (5GY 6/1) to pale olive (10Y 6/2) and appears homogenous in outcrop. It occurs as either massive deposits, as mottles within massive siltstone, or at the base of small-scale fining upwards sequences within finely laminated siltstone beds. The massive units below the paleosol contain large calcareous nodules 5-10 cm in diameter (at 85-96 cm) that fine upwards, along with spherical clay balls 0.5 to 2 cm in diameter (at 50-73, 85 to 96, and 105-114 cm) dispersed within the matrix. Coarse siltstone mottles are common in the paleosol (at 530 to 550 cm), positioned at 0 to -20 cm depth in the profile. One massive coarse siltstone is found above the paleosol (671-700 cm), and it contains

large (7-30 x 4-6 cm) elliptical, poorly cemented clay balls at its upper contact. Finely laminated intervals of alternating coarse siltstone and siltstone (at 268-296 cm below, and 710-850 cm above) are organized into cyclic fining upwards sequences, of which coarse siltstone is the base.

Siltstone Facies- Siltstone typically is greenish grey (5GY 6/1), dark greenish grey (5GY 4/1), or olive grey (5Y 4/1) in color, with one medium grey (N4) fine siltstone (350-498 cm) in the Wapadsberg section. This facies appears as a highly weathered, crumbling bed in the field. Siltstone units below the paleosol are massive, with the exception of one finely laminated interval in which several fining upwards sequences are found (Fig. 3). Massive siltstone close to the base of the section (at 73-85 and 140-210 cm) contains interspersed clay balls (ranging from 0.3-2 cm diameter). A single horizon in which massive brown-weathering (10YR 5/4) calcareous nodules (ranging from 1-4 m in diameter) occurs below the upper contact of a cross-bedded channel form sandstone (at 210 cm, Fig. 3). A massive siltstone with an exposure of a single basal carbonate nodule immediately underlies the paleosol (at 350-498 cm).

Above the paleosol, siltstone deposits are massive or finely laminated (mm-scale), exhibiting several fining upwards sequences. Homogeneous deposits (at 563-601, 603-671, and 702-712 cm, Fig. 3) contain fragmentary organic matter throughout, with a marked increase in the concentration above the paleosol. One horizon of elongate claystone balls (12 x 6 cm) (at 765 cm) and two horizons of regularly spaced root-cemented calcareous nodules (5 cm and 6 cm in diameter; at 808 and 849 cm, respectively) occur in the interval of finely laminated siltstone (at 710-850 cm).

Very Fine Sandstone Facies- The sandstone facies is greenish grey (5GY 4/1) to light olive grey (5Y 5/2) with very-fine sand (0.125-0.0625 mm) sized grains. It appears as a blocky or distinctly cross-bedded unit in the field. The facies occurs as meter-scale deposits with channel fill geometries overlain by siltstone on gradational or sharp contacts, and as discontinuous meter-scale lenses with poorly defined geometries below the paleosol. Channel-form sandstone exhibits well-defined 7-cm thick cross-bedding (best example from 210-276 cm, Fig. 3), and some include ripple (at 210-220 cm) or climbing ripple structures (mm-scale) (at 298-313 cm), mudclasts, mud chips, and/or clay balls. Mudclasts are concentrated along the lower contact of

the channel form, and mud chips and clay balls occur closer to the upper contact (50-210 cm). One channel body contains small-scale climbing ripple structures that are draped by organics and pyrite (at 298-313 cm), and represents the only occurrence of visible organic matter below the paleosol horizon. The discontinuous sandstone lenses below the paleosol are massive and contain mud clasts (~0.5 mm in diameter).

Above the paleosol, sandstone occurs only as discontinuous cm-scale lenses with small fragmented organic debris concentrated along bedding planes. These lenses occur in an interval of finely laminated siltstone with several thin fining upwards sequences (at 710-850 cm, Fig. 3). Ripples in sandstone also are present at the base of this interval (at 710-734 cm).

Sandy Siltstone Facies- Sandy siltstone is olive grey (5Y 4/1) and generally appears homogenous in the field, with few sedimentary structures visible where present. Three sandy siltstone intervals occur within this sequence, and each represents a different deposit. The lowermost deposit is massive and overlies the channel-form sandstone below the paleosol. Climbing ripples and organic clasts occur on a sharp contact (at 300-310 cm) between these units. The second deposit lies directly over the first on a sharp contact and makes up the base of a fining upwards sequence that transitions into coarse siltstone overlain by siltstone. The third deposit also is massive, but contains interspersed organic matter and well-rounded rooted clay balls (at 498-528 cm). The clay balls range in size from 25 x 10 cm to 100 x 30 cm, and rooting is concentrated at their tops. This interval is within part of the paleosol and is positioned at -20 to -50 cm depth within the profile (Fig 3).

White Claystone Facies- White claystone occurs in thin intervals that are pale yellowish orange (10YR 8/6) and easily distinguishable from the surrounding green lithologies (Fig. 5). The most prominent claystone layer caps the Wapadsberg Pass paleosol (at 550-563 cm, Fig. 3), and is 13 cm thick, finely laminated, and preserves impressions of *Glossopteris* leaves. One additional 2 cm thick layer occurs at -20 cm profile depth (at 528-530 cm). An interval of massive siltstone immediately overlying the paleosol contains two thin (5 mm thick) discontinuous white claystone laminae and a continuous white claystone layer (2 cm thick) in which *Glossopteris*-leaf impressions are preserved (at 574 and 584, and 601-603, respectively). One other claystone

layer is found higher upsection (at 700-702 cm, Fig. 3), and drapes a horizon of elliptical, poorly cemented clay balls. Rounded, elliptical to spherical clay balls are found throughout the Wapadsberg section and are 0.3-100 cm in diameter. These are distinguishable from surrounding matrix in the field, and weather moderate yellow brown (10YR 5/4). Unweathered claystone, inside these balls, ranges from moderate yellowish brown (10YR 5/4) to pinkish grey (5YR 8/1).

Petrographic Thin Sections

An examination of petrographic thin sections (Appendix 3) reveals that several different horizons can be identified in the paleosol profile. Primary structures include ripples, parallel bedding, and mm-scale soft-sediment deformation. These are partially destroyed due to phytoturbation and bioturbation. Organic matter debris, roots, pockets of coarse angular to rounded quartz clasts, and clusters of iron nodules also are observed. Throughout the profiles there is a texture that resembles brecciated clasts of fine material within a matrix of similar sized sediment, and is most prominent in the profile at -30 cm depth.

NWP- The top 20 cm of the NWP profile, below the white claystone, are siltstone mottled with coarse silt clasts. Primary structures in the top 2 cm are absent, homogenized by mm-scale bio-and-phytoturbation, with weak mm-scale bedding preserved between -8 cm to -20 cm depth. A horizon of strong iron staining coincides with a concentration of organic matter (OM) at -8 cm depth (Fig. 8 A). This horizon is visible in hand sample as a thin layer of degraded *Glossopteris* leaves preserved in a thin coating of white claystone, and fragmentary OM is intermixed throughout the -8 to -20 cm interval. Roots occur as thick amber features in these thin sections (Fig. 8 B). There is a concentration of coarser clasts between -20 to -30 cm depth and these are well homogenized, randomly iron-stained, and include ~50% intermixed singular rounded quartz grains (~1 mm) (Fig. 8 C). Also present are several geometrically (rectangular) shaped yellowish clasts (~5 mm) (Fig. 8 D). There is an additional concentration of OM at ~30 cm profile depth, below which is siltstone from -40 to -60 cm depth. Original parallel bedding and ripples are visible and well-preserved, some dark clasts of OM are present, and iron staining is exhibited as streaks and clusters of spherical iron nodules in this interval. Well-rounded to angular quartz grains (~0.5

to 1 mm) are interspersed at -50 to -60 cm depth as densely packed pockets that appear as mottles within the siltstone (Fig. 8 E). The relative proportion of quarts grains in these pockets is ~25%. These are texturally unique and are unrelated to primary bedding.

OWP- Thin sections from the two OWP profiles exhibit similar trends within the soil profile, but differ slightly. The profile is lithologically only siltstone. At the top of the paleosol is a concentrated horizon of organic matter (roots and leaves) oriented along bedding. From -10 to -30 cm depth micro-scale cross-bedding, ripple structures, and mottling occur (Appendix 3). Dispersed, 'stringy' organics are oriented along bedding planes and randomly oriented roots are observed as thick amber features through this part of the profile. Singular, isolated rounded quartz grains (~1 mm) are present, and are concentrated at -30 cm depth at a relative proportion of ~50%. Several rounded structures associated with OM and wrapped by bedding also are present within the -10 cm to -30 cm interval (Fig. 8 F). These contain the same type of yellowish clasts observed in the NWP profile at -20 to -30 cm depth (Fig. 8 D) and several unique textures that resemble an agglomeration of rounded clasts (~ 6 to 10 mm) with some interstitial mineral growth. The same clast types are intermixed in horizons of coarser material at -30 cm depth. Ripple structures are present at -50 cm depth, and OM is observed oriented parallel to bedding and capping several fining upwards sequences. Pockets of coarser sediment cross cut bedding. Isolated rounded quartz grains (~1 mm) are intermixed at -50 cm depth at a relative proportion of ~25%, and clusters of small spherical iron nodules (~0.1 mm) are present (Fig. 8 G). At the base of the paleosol profile, ripple structures are well-preserved, heavy iron staining occurs, roots and OM oriented along bedding planes is present, and there are clusters (~1x2 mm to ~2x3 mm) of iron nodules similar to those in other intervals. Rooting structures still are present at -70 cm depth, and are associated with pockets of coarser material (Fig. 8 H).

TOC and TOC:TON

Total organic carbon (TOC) ranges from a minimum value of 0.13 (NWP-2, Fig. 9) to a maximum value of 0.74 (OWP2-40, Fig. 9), and has an average value of 0.37 (Table 1). When TOC values are plotted versus paleosol depth for each locality, a positive excursion occurs in all profiles at -30 cm depth (Fig. 9). This increase is most prominent in the OWP2 profile (0.72), and

continues down section to -40 cm depth (0.74). Other positive spikes occur in NWP, to 0.42 at -8 cm depth, and in OWP1, to 0.46 at -70 cm depth. TON yielded a maximum value of 0.02 (NWP-50), and a maximum value of 0.11 (OWP2-40), with an average value of .06 (Table 2; Fig. 10).

Plots of TOC:TON versus paleosol depth yield similar profiles for each section sampled (OWP1, OWP2, and NWP) (Fig. 11). The ratios remain relatively consistent throughout the paleosol profile, ranging between 5.34 and 6.84 at OWP1 and OWP2. The average at OWP1 is 6.29, and at OWP2 the average is 6.24. The NWP ratios display larger variation ranging from 3.47 to 8.17, but remain for the most part between 5.5 and 7.0. A negative excursion to 3.47 occurs at -2 cm depth, and two positive excursions (7.71 and 8.17) occur at -8 cm and -50 cm depth, respectively. All TOC:TON values are less than 10, with an overall average of 6.26 (Table 3).

XRD Analysis

Spectra for each clay slide yielded similar patterns (Appendix 4). The spectral peaks were best fit to illite using Jade MDI 7 software and interpretation of spectra peak locations and intensities. Hence, there is no variation in clay type within the soil profile. Peaks for quartz, albite, muscovite, and clinochlore also were determined to be present and dominant in the spectra.

ICP-OES Analysis

Little variation across samples was shown in the suite of major-and trace-elements that were analyzed (Table 4). Major elements, including Al, Ca, Fe, K, Mg, Mn, Na, and Si, were reported as element-oxides and their concentrations fall within the expected range for sediments at this stratigraphic horizon analyzed by other researchers in the Karoo Basin (Coney et al., 2007). Several trace elements exhibited higher concentrations than expected, and include Co, Cr, Cs, Cu, Ni, V, Gd, and Nd. Trace elements exhibiting lower concentrations than expected include Eu, La, Sm, Yb and Y. Trace elements Ba, Sr, and Zn fell within their previously reported values, which span a large range of concentrations.

sample	depth (cm)	TOC	sample	depth (cm)	TOC	Sample	depth (cm)	TOC
NWPASH	0	0.19	OWP1-10	-10	0.42	OWP2ASH	0	0.41
NWPOH	-1	0.23	OWP1-20	-20	0.35	OWP2LH	-2	0.41
NWP-2	-2	0.13	OWP1-30	-30	0.47	OWP2-10	-10	0.43
NWP-4	-4	0.22	OWP1-40	-40	0.42	OWP2-20	-20	0.58
NWP-6	-6	0.23	OWP1-50	-50	0.40	OWP2-30	-30	0.72
NWP-8	-8	0.42	OWP1-60	-60	0.34	OWP2-40	-40	0.74
NWP-10	-10	0.22	OWP1-70	-70	0.46	OWP2-50	-50	0.41
NWP-15	-15	0.25	average		0.41	OWP2-60	-60	0.30
NWP-20	-20	0.24				OWP2-70	-70	0.24
NWP-25	-25	0.22				average		0.47
NWP-30	-30	0.30						
NWP-40	-40	0.23						
NWP-50	-50	0.20						
NWP-60	-60	0.14						
average		0.23						

Table 1- TOC values from CHNO-S analysis of all NWP, OWP1, and OWP2 localities.

sample	depth (cm)	TON	sample	depth (cm)	TON	sample	depth (cm)	TON
NWPASH	0	0.037	OWP1-10	10	0.076	OWP2ASH	0	0.077
NWPOH	1	0.043	OWP1-20	20	0.058	OWP2LH	2	0.075
NWP-2	2	0.036	OWP1-30	30	0.071	OWP2-10	10	0.063
NWP-4	4	0.031	OWP1-40	40	0.071	OWP2-20	20	0.086
NWP-6	6	0.037	OWP1-50	50	0.059	OWP2-30	30	0.107
NWP-8	8	0.055	OWP1-60	60	0.05	OWP2-40	40	0.11
NWP-10	10	0.029	OWP1-70	70	0.073	OWP2-50	50	0.066
NWP-15	15	0.04	average		0.065	OWP2-60	60	0.046
NWP-20	20	0.035				OWP2-70	70	0.041
NWP-25	25	0.037				average		0.075
NWP-30	30	0.048						
NWP-40	40	0.035						
NWP-50	50	0.024						
NWP-60	60	0.026						
average		0.037						

Table 2- TON values from CHNO-S analysis of all NWP, OWP1, and OWP2 localities.

sample	depth (cm)	TOC:TON	sample	depth (cm)	TOC:TON	sample	depth (cm)	TOC:TON
NWPASH	0	5.11	OWP1-10	-10	5.57	OWP2ASH	0	5.34
NWPOH	-1	5.30	OWP1-20	-20	6.09	OWP2LH	-2	5.49
NWP-2	-2	3.47	OWP1-30	-30	6.58	OWP2-10	-10	6.75
NWP-4	-4	6.94	OWP1-40	-40	5.87	OWP2-20	-20	6.69
NWP-6	-6	6.24	OWP1-50	-50	6.69	OWP2-30	-30	6.75
NWP-8	-8	7.71	OWP1-60	-60	6.84	OWP2-40	-40	6.70
NWP-10	-10	7.52	OWP1-70	-70	6.36	OWP2-50	-50	6.15
NWP-15	-15	6.30	average		6.28	OWP2-60	-60	6.41
NWP-20	-20	6.94				OWP2-70	-70	5.85
NWP-25	-25	5.89				average		6.24
NWP-30	-30	6.19						
NWP-40	-40	6.54						
NWP-50	-50	8.17						
NWP-60	-60	5.27						
average		6.26						

Table 3- TOC:TON values calculated for all localities (NWP, OWP1, and OWP2) using TOC and TON from CHNO-S analysis.

A.

sample	B	Ba	Be	Co	Cr	Cs	Cu	Ga	Ni	Pb	Sr	V	Zn	Dy	Eu	Gd	La	Nd	Sm	Yb	Li	Ti	Y	Mo
BIR	57	5	-0.2	48	366	5	114	11	159	24	107	317	81	4	0.3	20	-1	146	12	3	5	4852	14	15
NWPASH	62	857	3	10	61	857	31	15	19	56	369	123	53	5	1	15	57	171	11	2	39	3566	23	13
NWP-2	63	709	3	9	67	709	25	26	27	54	87	107	66	3	0	12	25	139	7	1	46	3585	16	12
NWP-4	55	679	3	16	63	679	19	27	27	45	104	97	73	4	0	13	20	138	7	1	47	3466	18	10
NWP-6	60	712	3	26	64	712	18	24	29	54	103	98	87	5	0	15	21	140	7	1	49	3393	18	10
NWP-8	61	708	4	9	69	708	19	25	32	50	98	111	140	4	0	15	23	138	8	2	54	3537	19	11
NWP-10	74	953	3	38	31	954	24	10	50	49	229	72	122	11	1	14	34	137	9	2	40	2926	23	21
NWP-15	49	740	4	6	36	740	12	17	13	39	206	71	68	5	0	14	39	142	10	2	36	3118	30	8
NWP-20	51	750	4	7	40	751	15	15	14	35	185	76	63	7	0	14	40	157	11	2	39	3377	31	9
NWP-25	55	744	5	20	45	744	20	18	21	41	184	83	76	13	0	16	51	170	12	2	41	3419	34	10
NWP-30	61	803	5	30	46	803	24	20	30	50	202	86	140	11	0	17	50	173	13	3	43	3562	35	10
NWP-40	59	687	4	14	46	687	19	21	26	40	177	86	156	7	0	16	40	155	11	2	42	3372	30	9
NWP-50	56	635	4	7	47	636	15	15	21	46	152	93	126	5	1	14	32	147	9	2	44	3489	26	8
NWP-60	64	667	4	40	59	668	17	17	42	61	89	126	118	6	0	15	35	149	9	2	54	3568	24	9
OWP1-10	49	672	2	9	37	672	16	7	9	26	315	66	60	4	1	10	26	128	9	1	42	3046	20	6
OWP1-20	50	734	2	9	41	735	14	7	11	33	356	63	69	4	0	11	27	131	7	1	43	3074	21	6
OWP1-30	48	708	2	8	37	708	18	13	8	36	289	70	87	4	0	11	31	129	9	1	43	2821	21	6
OWP1-40	49	719	2	10	47	720	12	17	9	27	147	78	41	2	0	7	15	105	5	1	43	2704	15	4
OWP1-50	59	583	2	13	229	584	19	18	41	29	159	88	102	4	1	13	29	123	10	2	54	2803	20	8
OWP1-60	61	631	3	11	46	631	15	5	20	34	177	88	96	4	0	13	30	134	9	2	56	3038	20	7
OWP1-70	55	563	2	8	46	564	18	4	13	21	172	81	79	4	1	12	25	120	9	1	49	2739	18	6
OWP2-ASH	50	887	2	10	46	887	4	14	2	11	179	118	17	1	0	5	20	124	4	0	19	3359	9	11
OWP2-LH	74	819	2	9	47	819	18	13	20	22	141	92	117	3	0	15	24	116	9	1	51	2816	16	9
OWP2-10	65	827	2	4	48	828	16	13	13	30	166	84	76	3	1	14	21	120	7	1	49	3049	15	15
OWP2-20	66	832	3	6	64	833	15	13	22	41	125	104	127	5	0	14	27	128	10	2	52	2942	22	14
OWP2-30	55	777	2	5	46	777	36	13	7	0	125	83	42	3	0	10	24	120	7	1	47	2909	18	8
OWP2-40	90	750	3	4	55	750	16	25	13	38	103	119	101	7	1	22	28	145	14	3	48	3107	33	14
OWP2-60	60	706	2	6	50	706	23	17	9	30	165	90	73	3	1	12	22	123	9	1	51	3062	17	9
OWP2-70	73	759	3	40	49	759	21	14	32	65	120	118	95	7	0	16	51	155	12	2	48	2917	22	13

B.

	B	Ba	Be	Co	Cr	Cs	Cu	Ga	Ni	Pb	Sr	V	Zn	Dy	Eu	Gd	La	Nd	Sm	Yb	Li	Ti	Y	Mo
av. NWP	59	742	4	18	52	742	20	19	27	48	168	95	99	7	0	15	36	150	10	2	44	3414	25	11
av. OWP1	53	659	2	10	69	659	16	10	16	29	231	76	76	4	0	11	26	124	8	1	47	2889	19	6
av. OWP2	67	795	2	10	51	795	19	15	15	30	140	101	81	4	0	13	27	129	9	1	46	3020	19	11
av. (total)	60	736	3	14	56	736	18	16	21	38	176	92	88	5	0	13	31	138	9	2	45	3170	22	10

Table 4- A.- Major- and trace-element abundance results from ICP-OES analysis. Major-element abundances are in wt. % and trace-element abundances are in ppm. B- Average trace-element abundances for all paleosol localities (NWP, OWP1, and OWP2).

The Ba/Sr values also were calculated using ICP-OES trace element results for all of the paleosol samples (NWP, OWP1, and OWP2) and plotted v. paleosol profile depth (Fig. 12). The ratio ranges from 2.32 (at 0 cm depth) to 8.12 (at -2 cm depth) for NWP, from 2.06 (at -20 cm depth) to 4.91 (at -40 cm depth) for OWP1, and from 4.29 (at -60 cm depth) to 7.24 (at -40 cm depth) for OWP2. The Ba/Sr trend for NWP is slightly different than those for OWP1 and OWP2. The NWP Ba/Sr shifts from the minimum value to the maximum value within the top 2 cm of the profile. Values then remain relatively high until -8 cm, and then drop to 4.17 (from 7.25) at -10 cm depth. The Ba/Sr shows little variation between -10 cm and -50 cm, but exhibits a positive shift from 4.19 to 7.19 at -60 cm base of the profile. OWP1 and OWP2 exhibit comparable trends to each other, with an overall increase from the tops of their profiles (2.13 at -10 cm for OWP1 and 4.94 at 0 cm for OWP2) to a positive spike at -40 cm (OWP1 to 4.91, OWP2 to 7.24). Below this spike, OWP1 values decrease to a medial value of 3.28 at the -70 cm profile base. OWP2 exhibits a strong negative shift at -60 cm depth (to 4.29) before returning to a medial value of 6.34 at the -70 cm depth profile base.

XRF Analysis

Data for major element wt% abundances and several trace element abundances (ppm) were generated using XRF analysis (Table 5). Little variation across samples was shown in the suite of major-and trace-elements that were analyzed. Major elements, including Al, Ca, Fe, K, Mg, Mn, Na, and Si, were reported as element-oxides and their concentrations fall within the expected range for sediments at this stratigraphic horizon analyzed by other researchers in the Karoo Basin (Coney et al., 2007). Several trace elements exhibited higher concentrations than expected, and include Co, Cr, Cs, Cu, Ni, V, Gd, and Nd. Trace elements exhibiting lower concentrations than expected include Eu, La, Sm, Yb and Y. Trace elements Ba, Sr, and Zn fell within their previously reported values, which span a large range of concentrations.

Soil Molecular Weathering Ratios

Base loss- The base loss plot exhibits two distinct groups of similar trends, one of Na and Ca, and one of Mg and K (Fig. 13; Table 6). The trends between these two groups, however, are dissimilar, and the base loss profile shows higher degrees of leaching of Ca and Na

A.

Sample	Al2O3 (%)	CaO (%)	Fe2O3 (%)	K2O (%)	MgO (%)	MnO (%)	Na2O (%)	P2O5 (%)	SiO2 (%)	TiO2 (%)	Sum (%)
NWP ASH	19.624	0.996	5.542	4.301	1.694	0.038	0.862	0.184	65.801	0.748	99.79
NWP-2	19.169	0.758	5.519	4.055	1.956	0.068	0.922	0.09	66.609	0.723	99.867
NWP-4	17.716	0.914	5.905	3.615	1.951	0.064	1.284	0.109	67.598	0.705	99.86
NWP-6	17.683	0.915	6.405	3.68	1.994	0.127	1.131	0.099	67.133	0.688	99.855
NWP-8	18.657	0.905	6.521	3.96	2.16	0.069	1.162	0.097	65.607	0.713	99.85
NWP-10	16.075	1.452	4.622	3.436	1.309	0.141	1.892	0.19	70.099	0.615	99.831
NWP-15	16.844	1.794	4.234	3.773	1.476	0.044	1.702	0.384	68.946	0.641	99.839
NWP-20	17.199	1.788	4.192	3.925	1.541	0.103	1.582	0.45	68.365	0.688	99.834
NWP-25	19.624	0.996	5.542	4.301	1.694	0.038	0.862	0.184	65.801	0.748	99.79
NWP-30	17.016	2.011	4.568	3.991	1.619	0.242	1.598	0.612	67.485	0.681	99.823
NWP-40	16.992	1.745	4.945	3.943	1.662	0.103	1.652	0.455	67.658	0.69	99.844
NWP-50	17.562	1.449	4.843	4.108	1.77	0.037	1.47	0.249	67.629	0.714	99.831
NWP-60	17.973	0.956	6.248	4.45	2.096	0.125	0.832	0.123	66.334	0.714	99.853

B.

Sample	Ba (PPM)	Cr (PPM)	Zn (PPM)	Sr (PPM)	Y (PPM)	Zr (PPM)	Rb (PPM)	Nb (PPM)
NWP ASH	1015	85	45	431	30	205	201	22
NWP-2	805	76	61	100	22	131	192	17
NWP-4	777	73	65	119	23	128	174	18
NWP-6	758	68	81	116	24	120	173	18
NWP-8	798	84	139	112	24	125	184	20
NWP-10	936	44	96	253	27	275	145	18
NWP-15	816	46	64	218	36	245	163	21
NWP-20	862	50	60	203	36	234	180	23
NWP-25	833	55	72	202	42	221	174	25
NWP-30	827	53	126	206	39	231	180	23
NWP-40	778	58	159	193	35	213	177	24
NWP-50	706	56	123	174	33	225	187	23
NWP-60	772	82	115	101	31	156	218	22
average	826	62	91	194	31	196	178	21

Table 5- Major- and trace-element abundance results from XRD analysis. A.- Malor element abundance results (wt%), normalized to 100. B.- Trace element abundance results (ppm).

than of Mg and K. Base Loss values range from 1.19 (at 0 cm and -25 cm) to 3.17 (at -10 cm) for Na,from 1.19 (at -2 cm) to 3.36 (at -30 cm) for Ca, from 3.37 (at -10 cm) to 4.80 (at -8 cm) for Mg, and from 3.48 (at -4 cm) to 4.23 (at -60 cm) for K. Ca and Na remain relatively constant at minimum values for the top 8 cm of the profile, and then exhibit a sharp positive excursion at -10 cm depth (Na- 1.68 to 3.17, Ca- 1.45 to 2.69). Values do not fluctuate widely between -10 and -20 cm depth, but shift to minimum values at -25 cm (Na- 1.19, Ca- 1.52), before returning to similar values at -30 cm (Na- 2.42, Ca- 3.36). There is an overall decrease in values from -30 cm to the -60 cm (Na- 1.20, Ca- 1.53) base of the profile. Mg and K remain relatively constant throughout the entire profile, with Mg exhibiting a single negative excursion at -8 cm to -10 cm depth (from 4.80 to 3.37), and K exhibiting a small negative excursion at -4 cm depth (from 3.80 to 3.48).

Clayeyness and Mineral Assemblage Stability- When plotted against paleosol profile depth for the NWP section, clayeyness (Al/Si), and mineral assemblage stability (Fe/ K) exhibit similar trends (Fig. 14 A and B; Table 6). Clayeyness values range from 0.14 to 0.18, with the minimum occurring at -10 cm, and the maximum value at the white claystone (0 cm) and -25 cm. Mineral assemblage stability values range from 0.63 to 1.03, with the minimum occurring at -20 cm, and the maximum value at -6 cm. The trends for base loss and clayeyness values are relatively high (base loss- 69.74 to 72.46, clayeyness- 0.15 to 0.18) in the upper 8 cm of the soil, and undergo a sharp negative shift (base loss to 62.92, clayeyness to 0.14) at depth. Values are close to the minima, and remain low until -25 cm depth where a positive excursion (base loss from 63.00 to 71.34, clayeness from 0.15 to 0.18) occurs at this horizon. A return to higher values occurs at -30 cm (base loss- 61.61, clayeyness- 0.15). A gradual increase in values occurs from -30 cm to -60 cm until higher values are reached at the base of the profile (base loss- 69.40, clayeyness- 0.16).

Mineral-assemblage stability values exhibit a slightly different trend (Fig. 14 B). The maximum positive excursion occurs at -6 cm (1.03), with relatively high values at -4 and -8 cm as well (0.96 and 0.97, respectively). A swing to the minimum value in the profile at -20 (0.63) cm is followed by a positive excursion at -25 cm (0.76), paralleling those observed for base loss and

clayeyness. There is a similar overall increase in values between -30 and -60 cm (from 0.68 to 0.83), but mineral-assemblage stability exhibits a small positive excursion at -40 cm (from 0.68 to 0.74) during this increase.

Calcification, Salinization, Mineralogical Maturity- When plotted against paleosol profile depth, calcification ((Ca+Mg)/Al), salinization ((K+Na)/Al), and mineralogical maturity (Si /Al) exhibit similar trends (Fig. 15 A-C; Table 6). Calcification values range from 0.311 to 0.456, with the minimum occurring at two horizons (white claystone at 0 cm and -25 cm) and the maximum value at -30 cm in the profile. Salinization values range from 0.28 to 0.84, with the minimum occurring at -60 cm, and the maximum value in the white claystone (0 cm) and -10 cm depth. Mineralogical maturity values range from 5.69 to 7.40, with the minimum occurring at the white claystone and the maximum value at -10 cm depth.

Salinization and mineralogical maturity exhibit remarkably similar trends with depth through the paleosol profile. Values are relatively low (salinization- 0.31 to 0.34, mineralogical maturity- 5.690 to 6.475) within the upper 8 cm of the profile. The beginning of a small excursion occurs at -4 cm, but returns to lower values at -8 cm depth. The greatest positive excursion occurs at -10 cm depth (salinization from 0.33 to 0.42, mineralogical maturity from 5.97 to 7.40), and decreases to the maximum negative value at -25 cm in the profile (salinization- 0.31, mineralogical maturity- 5.69). Values increase at -30 cm (0.46 for salinization, 6.73 for mineralogical maturity) and then decrease steadily until the base of the profile (reaching 0.39 for salinization and 6.26 for mineralogical maturity).

The trend for calcification (Fig. 15 C) is similar to that of salinization and mineralogical maturity for -15 cm and below. The upper 10 cm exhibits slightly different behavior. Values increase steadily from 0.31 to 0.38 from the white claystone (0 cm) down to -8 cm depth, drop minimally at -10 cm depth (0.37), and then increase again at -15 cm depth (0.42). Values at -15 to -20 cm are similar, below which a slight negative excursion (from 0.42 to 0.31), occurs, similar to the ones observed for calcification and salinization values.

A.

	molar element abundance						
sample	Na	Al	K	Ca	Si	Fe	Mg
NWP ASH	0.01	0.19	0.05	0.02	1.10	0.03	0.04
NWP-2	0.01	0.19	0.04	0.01	1.11	0.03	0.05
NWP-4	0.02	0.17	0.04	0.02	1.13	0.04	0.05
NWP-6	0.02	0.17	0.04	0.02	1.12	0.04	0.05
NWP-8	0.02	0.18	0.04	0.02	1.09	0.04	0.05
NWP-10	0.03	0.16	0.04	0.03	1.17	0.03	0.03
NWP-15	0.03	0.17	0.04	0.03	1.15	0.03	0.04
NWP-20	0.03	0.17	0.04	0.03	1.14	0.03	0.04
NWP-25	0.01	0.19	0.05	0.02	1.10	0.03	0.04
NWP-30	0.03	0.17	0.04	0.04	1.12	0.03	0.04
NWP-40	0.03	0.17	0.04	0.03	1.13	0.03	0.04
NWP-50	0.02	0.17	0.04	0.03	1.13	0.03	0.04
NWP-60	0.01	0.18	0.05	0.02	1.10	0.04	0.05

B.

sample	Na/Ti	K/Ti	Ca/Ti	Mg/Ti	(Ca+Mg) / Al	(K+Na)/Al	Al / Si	Si / Al	Fe / K
NWP ASH	1.19	3.90	1.52	3.59	0.31	0.31	0.18	5.69	0.76
NWP-2	1.31	3.80	1.19	4.29	0.33	0.31	0.17	5.90	0.80
NWP-4	1.88	3.48	1.48	4.39	0.37	0.34	0.15	6.48	0.96
NWP-6	1.69	3.63	1.51	4.59	0.38	0.33	0.16	6.44	1.03
NWP-8	1.68	3.77	1.45	4.80	0.38	0.33	0.17	5.97	0.97
NWP-10	3.17	3.79	2.69	3.37	0.37	0.42	0.14	7.40	0.79
NWP-15	2.74	3.99	3.19	3.65	0.42	0.41	0.14	6.95	0.66
NWP-20	2.37	3.87	2.96	3.55	0.42	0.40	0.15	6.75	0.63
NWP-25	1.19	3.90	1.52	3.59	0.31	0.31	0.18	5.69	0.76
NWP-30	2.42	3.97	3.36	3.77	0.46	0.41	0.15	6.73	0.68
NWP-40	2.47	3.88	2.88	3.82	0.43	0.41	0.15	6.76	0.74
NWP-50	2.12	3.90	2.31	3.93	0.40	0.39	0.15	6.53	0.70
NWP-60	1.20	4.23	1.53	4.65	0.39	0.34	0.16	6.26	0.83
average	1.96	3.85	2.12	4.00	0.38	0.36	0.16	6.43	0.79

Table 6- A- XRF wt % values converted to molar element abundances. B- Calculated values of base loss, clayeyness, mineral assemblage stability, calcification, salinization, and mineralogical maturity for the NWP paleosol profile, using molar element abundances.

CAI-K

CAI-K values range from 73.03 to 86.88, with an average value of 80.03 (Table 7). The CIA-K values over depth through the paleosol profile (Fig. 16) reveal several horizons where CAI-K values are high, relative to the average. Between 0 and -8 cm, the CAI-K ranges from 82.44 to 86.88 (the highest value for the paleosol). Values become immediately lower at -10 cm depth, where they remain between 73.54 and 74.61 until a depth of -20 cm. Another positive spike to 85.87 occurs at -25 cm, after which the CAI-K returns to 73.03 at – 30 cm (the lowest value observed in the paleosol). From -30 cm to the base of the paleosol at -60 cm, the CAI-K increases steadily until it reaches another maximum of 85.26 at -60 cm.

Discussion

The Karoo Basin contains the most extensive, purportedly continuous continental sedimentary record that spans the Permian through the Triassic. Thus, it has been the subject of many studies concentrating on the terrestrial P-Tr mass extinction event. Despite the importance of paleosols and their potential use for extrapolating paleoclimate, very few studies in the Karoo have focused on them, to date (Smith, 1995; Retallack et al., 2003; Smith and Botha, 2005; Botha and Smith, 2006). Of these studies, none offer any high-resolution analysis of paleosols. Currently, the classification scheme developed for Late Permian and Early Triassic paleosols by Retallack et al. (2003) is the most detailed. However, it does not offer any distinctive features or set of criteria by which to identify each paleosol-type, as the criteria presented are limited to differences in color or sediment character of the lithology (sandstone v. siltstone). Both of these features may vary on a local or regional scale and, therefore, are not an acceptable basis on which to define or distinguish different types of soils. Additionally, Retallack et al.'s (2003) classification scheme describes some of the Permian paleosols using several, contradictory soil-types and needs to be revised. This lack of clarity, and the absence of classifications from other studies, exemplifies the need for more distinct and detailed descriptions of these paleosols. Hence, this study offers the first high-resolution characterization of a paleosol in the Karoo Basin, near the PTB, that also provides its sedimentological context.

Paleosol Interpretation

	wt %				molar element abundance				molar ratio	
Sample	Na2O	Al2O3	K2O	CaO	Na	Al	K	Ca	Al / (Al+Ca+Na+K)	CIA-K
NWP ASH	0.86	19.62	4.30	1.00	0.01	0.19	0.05	0.02	71.34	85.87
NWP-2	0.92	19.17	4.06	0.76	0.01	0.19	0.04	0.01	72.46	86.88
NWP-4	1.28	17.72	3.62	0.91	0.02	0.17	0.04	0.02	69.74	82.44
NWP-6	1.13	17.68	3.68	0.92	0.02	0.17	0.04	0.02	70.20	83.38
NWP-8	1.16	18.66	3.96	0.91	0.02	0.18	0.04	0.02	70.40	83.99
NWP-10	1.89	16.08	3.44	1.45	0.03	0.16	0.04	0.03	62.92	73.65
NWP-15	1.70	16.84	3.77	1.79	0.03	0.17	0.04	0.03	62.41	73.54
NWP-20	1.58	17.20	3.93	1.79	0.03	0.17	0.04	0.03	63.00	74.61
NWP-25	0.86	19.62	4.30	1.00	0.01	0.19	0.05	0.02	71.34	85.87
NWP-30	1.60	17.02	3.99	2.01	0.03	0.17	0.04	0.04	61.60	73.03
NWP-40	1.65	16.99	3.94	1.75	0.03	0.17	0.04	0.03	62.58	74.26
NWP-50	1.47	17.56	4.11	1.45	0.02	0.17	0.04	0.03	64.90	77.66
NWP-60	0.83	17.97	4.45	0.96	0.01	0.18	0.05	0.02	69.40	85.26

Table 7- CIA-K values calculated from XRF wt% data converted to molar element abundance.

An interpreted soil is found in the stratigraphic section at Wapadsberg Pass, and the paleosol profile includes three facies, the white claystone, coarse siltstone, and siltstone. The upper limit of the paleosol was placed at the top of a 13 cm thick layer of white claystone with impressions of *Glossopteris* leaves. The base of the paleosol, with a total thickness of ~70 cm below the base of the white claystone horizon, was marked by the lowest extent of *in situ* rooting structures. The entire paleosol is greenish-grey (5GY 6/1) and fairly homogeneous in outcrop, except for a 2 cm thick rooted white claystone deposit at -20 cm depth, rounded claystone balls concentrated at ~30 cm depth (and present until -50 cm depth), and some iron staining throughout. Two lithologies and several biogenic and abiogenic features occur within this ~70 cm paleosol interval (Fig. 3). Siltstone with coarse siltstone mottles underlies the claystone at 0 cm and contains remnants of poorly preserved *Glossopteris* leaves and *Vertebraria* roots. Below this, at -20 cm depth, is a thin (2 cm) rooted white claystone which overlies an interval of coarse siltstone extending to -50 cm depth. Interspersed organic matter and several large rooted clay balls occur. The remaining paleosol profile is a massive and homogenous siltstone with rooting structures that penetrate to ~70 cm depth.

The poorly-developed Wapadsberg Pass paleosol does not match any existing descriptions of Karoo paleosols, or fit the soil classification scheme of Retallack et al. (2003). This paleosol has been classified as an inceptisol, due to its lack of well-defined horizons, the absence of a significant argillic horizon, and the indication that little development has occurred by the presence of relict primary structures (Retallack, 2001). The characteristics that distinguish this paleosol from those described that are similar to it are the absence of calcareous nodules at depth, the absence of banded clay, the greenish-grey color, and the deep rooting structures of *Glossopterids* (i.e., *Vertebraria*). The NWP paleosol also is unique for several other reasons. It is the only paleosol reported, to date, that contains a white claystone layer from which detrital zircons also have been recovered. Hence, this particular soil exhibits evidence of volcanic clast influence. In addition, a well-preserved autochthonous forest-floor megafloral assemblage was found at all three separate, stratigraphically isochronous paleosol localities (NWP, OWP1, and

OWP2) (Reid et al., 2007; Prevec et al., in press) The spatial separation of these localities allows for the investigation of local (~1 km) variation across the paleosol horizon (geochemical results for OWP1 and OWP2 outcrops pending). The fossil-plant assemblage collected from this paleosol is unique to the basin and is the youngest autochthonous assemblage recovered from the Karoo, to date. As such, this flora represents the plants that lived across a landscape pior to the PTB in Gondwana. This assemblage includes the youngest *Glossopteris* collected in the basin that has been reported, to date.

The white claystone layer capping the NWP paleosol has been interpreted to be derived from a volcanic ash deposit (tuffite), based on its stark contrast to the surrounding sediments and the character of its lithology. The tuffite occurs as dispersed isolated clasts within the fine matrix and is distributed in irregular pockets which cross-cut bedding. The claystone layer at 0 cm and the claystone balls at -30 cm depth include intermixed sand-sized quartz grains, a size difference that is rare for fluvially generated sediments. These quartz grains, visible under petrographic thin section, are interpreted to be intermixed tuffite, characterized as a mix of well-rounded to angular transparent quartz clasts. All three paleosol sites examined contain this tuffite within their profiles, concentrated around -20 to -30 cm and -60 to -70 cm depth. The concentrations of tuffite and coarser sediment that cross cut bedding are interpreted to be in-filled burrows based on their structure. The conclusion that these quartz clasts represent a tuffite is based on the mixed degree of their rounding, the presence of the white claystone capping the paleosol profile, and recovery of detrital zircons from this white claystone layer.

Several other distinct features and textures were observed under thin section. Isolated yellowish clasts were observed in the NWP and OWP thin sections, at -20 to -30 cm depth. These are thought to possibly be bone fragments because of their shape and color (Neil Tabor, SMU, personal communication), but also could represent siltstone rip-up clasts. There also is a ‘brecciated’ texture observed in all three profiles, which is interpreted to result from the formation and reworking of soil peds.

Sedimentological Context

The paleosol at New Wapadsberg Pass occurs ~70 m below the purpored PTB, within the Beaufort Group. The fluvial and interfluvial deposits of the Beaufort Group capture both aggradational and degradational floodplain sediments, visible within the ~9 m section at New Wapadsberg Pass examined for the present study. Aggradational landscapes are represented by fining-upwards sequences of sandstone or siltstone that reach up to several meters in thickness, and degradational landscapes, triggered by the development of meandering rivers, are marked by channel fill deposits of sandstone barforms or siltstone plugs (Reid et al., 2007).

The NWP paleosol resides ~5 m up in the NWP section measured for the present study, and there is a noticeable difference in depositional style above and below it. The sequence above the paleosol is dominated by massive siltstone and fining upwards sequences that suggest mostly aggradational deposition. Most deposits below the paleosol are considered to be degradational in nature based on their geometries and the inclusion of abundant mud clasts, mud chips, and rounded ash balls. Paleosol development marks periods of landscape stasis and stability on the floodplain (Reid et al., 2007). These periods of stasis and soil formation record the environmental and climatic conditions that existed and offer many tools for interpreting the paleoenvironment during paleosol development.

The NWP paleosol likely developed proximal, but not adjacent to, a channel margin. Paleosol maturity across floodplains increases with the distance from the fluvial channel, and is controlled by flood recurrence interval, flood intensity, and the rate at which accommodation space is created (Sheldon and Tabor, 2009). Typically, there is an observed sequence of channel-margin entisols or protosols to better developed paleosols, such as inceptisols, on floodplains (Retallack, 2001; Sheldon and Tabor, 2009). Based on this progression, the classification of the NWP paleosol as a wetland inceptisol, and its sedimentological context, the NWP paleosol is concluded to have developed on a floodplain.

Clay Minerals

The clay minerals produced in a soil profile are dependent on the parent material composition, the time taken for soil formation, the ambient temperature, and the seasonality of rainfall (Retallack, 2001). The composition of the paleosol clay-sized fraction at NWP supports

an interpretation that illite is the predominant clay mineral within the profile. Illite is formed either as a product resulting from the weathering of muscovite and feldspar or by illitization of the soil clay minerals during diagenesis. Illite from weathering processes forms under dry, temperate climate regimes (Douchafour, 1977; Sheldon and Tabor, 2009). It is a relatively unstable clay mineral and indicates, especially in combination with chlorite (clinochlore is present in the NWP and OWP paleosols) that little chemical weathering or alteration of the soil occurred (Hunt, 1972). This agrees with the classification of the Wapadsberg Pass paleosol as an inceptisol. Illite is observed to be the most prominent clay mineral in young soils of desert (arid) regions experiencing strong wet-dry seasonality (Retallack, 2001, p.95). Illite also can be the product of illitization, which can occur from alteration of the paleosol sediments after burial and during diagenesis. This process also may be responsible for generating the illite fraction of the NWP paleosol.

There is a perceived discrepancy between the presence of illite, an indicator of low weathering, dominating the soil clay fraction and the very high CIA-K value indicative of abundant weathering of the paleosol. Pure illite does have CIA-K values that range from 75 and 85 (Scheffler et al., 2006; Sheldon and Tabor, 2009). Hence, this is not necessarily an issue. However, the clay-mineral fraction of this locality is likely a result of illitiization during diagenesis. The NWP area was intruded by numerous Jurassic dolerite dikes (Johnson et al., 2006) which outcrop ~0.5 km NW and ~80 m upsection from the NWP paleosol, along R61 (S31˚55'47.4", E24˚53'11.3"). There are visible alteration halos, in response to contact metamorphism, surrounding the dikes that evidence additional heating of the New Wapadsberg Pass area. The NWP paleosol lies outside of the alteration halos, but is proximal enough that additional heating of the sediments would have occurred during-or-post diagenesis, resulting in the illitization of the clay fraction Temperatures as low as 50˚C result in illitization (Lahann, 1980), and it is reasonable to assume similar or higher temperatures could be generated by the dikes. Hence, illite is not a conclusive indicator of climatic conditions at the time of soil formation because it is not a product of original weathering in the NWP paleosol.

Proxy Trends

The paleoenvironmental proxies can be used to reconstruct some of the general climatic conditions present during the Late Permian of the Karoo Basin. The TOC, CIA-K, and the soil molecular weathering ratio patterns all correlate well, and can be used to extrapolate several paleoenvironmental conditions. These include the environment in which the paleosol developed and rough estimates of climate conditions.

TOC:TON- The TOC:TON values calculated for the NWP and OWP profiles all plot below 10, representing an algal signature (Scheffler et al., 2006). One possible explanation for this observed algal signature in the terrestrial paleosol is that this soil developed in wetland conditions with a high water table. Wetland soils are likely to be inhabited by a greater number of algae relative to better drained soils, and a high concentration of freshwater algae could be abundant enough to have generated the signature recorded at Wapadsberg Pass.

TOC- The plot of total organic carbon versus paleosol profile exhibits a significantly higher concentration of C at -30 cm depth for all three locations. The only mechanisms for accumulation of OM (C) at depth within a soil would require that (1) sediment covered OM of an older soil surface (O-horizon), or (2) the translocation of OM (and Fe-Al complexes in acid-rich soils) to a spodic horizon had occurred (Neil Tabor, SMU, pers. communic., 3/2010). No increase in either Fe or Al is observed at this -30 cm depth horizon to indicate the presence of a spodic horizon. Hence, this concentration of C is interpreted to represent the O-horizon (reworked to several cm depth during subsequent sedimentation) of an older soil which was then overprinted by another, younger soil. This indicates that the NWP profile is not a single soil, but represents a stacked paleosol profile with soil surfaces at 0 cm and -25 cm depth. When compared to the observed stratigraphy of the NWP paleosol, this interpretation is further supported by the presence of a white claystone at -20 cm depth capping the interpreted -25 cm surface.

CIA-K- The pattern observed in the CIA-K values and the soil molecular weathering ratios v. profile depth correlates well to the pattern of TOC v. profile depth. Hence, the CIA-K and soil molecular weathering-ratio plots also support a stacked paleosol interpretation, as they exhibit significant excursions in their profiles at the same depths.

The CIA-K exhibits maximum values at 0 cm and -25 cm depth, which are interpreted to represent soil-surface horizons based on the expectation that soil surfaces are subject to the greatest degree of weathering (Fig. 16). There also is likely to be an effect on the CIA-K profile from any reworking of surface sediments and OM into the profile by aggradational floodplain deposits over these horizons. Similar increasing trends in CIA-K are observed below the maximum values at both of the interpreted soil surfaces. The -30 cm horizon, where the positive spike in TOC occurs, however, yields the lowest CIA-K value in the profile. This is interpreted to represent a spodic horizon, based on its shallow placement beneath the interpreted older soil. The same decrease in CIA-K value is observed just below the 0 cm top of the paleosol profile, where the soil surface is well defined by the forest-floor O-horizon. Hence, this phenomenon is likely due to the accumulation of translocated or reworked OM and associated sub-surface soil micro-organisms at shallow depths below each soil surface. Fluctuations in the CIA-K also could be attributed to changes in lithology within the plaeosol profile, but this explanation is not favored because there is no observed lithologic change between 0 and -8 cm or -20 and -50 cm depth.

Soil Molecular Weathering Ratios- Each calculated soil molecular weathering ratio acts as a proxy for different pedogenic conditions. Base loss, defined as (Ca, Mg, Na, K)/Ti, is used as a measure of the amount of leaching undergone by a soil (Sheldon and Tabor, 2009). Base elements including Ca, Mg, Na, and K all are leached relative to Ti, which accumulates within the soil profile (Sheldon and Tabor, 2009). The Mg and K profiles show little fluctuation in leaching except for a single, sharp decrease in Mg-loss from -8 cm to -10 cm depth (Fig. 13). There are relatively low, similar degrees of leaching for Na and Ca at 0 cm and -25 cm that correspond to the interpreted soil surfaces. The low base loss at these surfaces both are underlain by increases in Na and Ca leaching, and these are attributed to the presence of the water table at these intervals during soil formation. A high wetland water table would preferentially mobilize and leach Ca and Na from the profile, as they are more water soluble than Mg and K (Sheldon and Tabor, 2009), resulting in the observed proxy increase.

Clayeyness, defined as Al/Si, is a proxy for hydrolysis and clay-mineral formation as Al accumulates in clays relative to the siliceous parent material (Sheldon and Tabor, 2009).

Maximum clayeyness values in the NWP paleosol occur at 0 cm and -25 cm depth, which correspond to the interpreted soil surfaces within the profile. It is unlikely that argillic-like horizons would form at a soil surface, as clays typically are translocated to horizons at depth within soil profiles (Sheldon and Tabor, 2009). Hence, the positive spikes indicating the increased presence of clay are attributed to the corresponding ash which is incorporated at these horizons. The observed trend for clayeyness also supports the stacked paleosol interpretation.

Salinization, defined as (K+Na)/Al, indicates the abundance of salts within any soil profile (Sheldon and Tabor, 2009). Alkali elements, like K and Na, typically are mobile but become trapped and accumulate in soluble salts that are not removed from the soil (Sheldon and Tabor, 2009). Salinization can be used as a measure of mean annual temperature (MAT), as the accumulation of salts is common in arid and desert paleosols where there is little water to remove them (Sheldon and Tabor, 2009). Increasing salinization implies an increasing MAT based on the relationship between increasing temperature and aridity. However, the use of salinization as a proxy for MAT in soils older than the Mesozoic is cautioned because salts are lost during diagenesis and leave only evaporate psuedomorphs (Sheldon and Tabor, 2009). While salinization may not be a reliable indication of MAT for the NWP paleosol, due to the exacerbation of diagenesis by the surrounding dolerite dikes, it brings up another point relevant to a paleoclimate interpretation. Temperature and aridity are not implicitly linked. Desert soils can exhibit relatively low MAT despite their maximum temperatures, because these only occur daily and seasonally (Sheldon and Tabor, 2009).

The soil molecular weathering ratio patterns show similar sharp shifts and trends to CIA-K, and can be applied as additional proxies to assess paleoenvironmental conditions. The ratio plots, with the exception of base loss, fall into two groups (Fig. 14 and 15). One group includes clayeyness and mineral assemblage stability, and the other includes calcification, salinization, and mineralogical maturity. These groups exhibit inverse trends from each other, and all of the indices show a prominent positive or negative excursion at -25 cm. Similar trends exist between 0 cm to -20 cm depth and from -25 cm depth to the base of the soil profile.

Ba/Sr Ratio- The Ba/Sr ratio is a proxy for leaching of trace elements, resulting from weathering intensity (Sheldon and Tabor, 2009). Ba and Sr both are alkali earth elements, have similar atomic radii, and similar affinities. However, Sr is significantly more soluble and easily leached than Ba meaning that higher Ba/Sr ratios indicate greater soil leaching (Sheldon and Tabor, 2009). Soils that are leached of trace elements exhibit lower Ba/Sr ratios at the tops of their profiles, and relatively higher Ba/Sr ratios at the B-horizon, if present, within their profiles (Sheldon and Tabor, 2009). The NWP and OWP paleosol profiles have minimum or near minimum Ba/Sr ratios at their surfaces. However, the NWP paleosol profile Ba/Sr ratio swings immediately to maximum values at -2 cm depth (Fig. 12). Besides this excursion, there are no discernable trends in the Ba/Sr ratio that would imply either leaching of the soil or the presence of a well-developed B-horizon. Because the New and Old Wapadsberg Pass paleosols are inceptsols, a soil type that does not have a well-developed B-horizon, the Ba/Sr ratio as a proxy for leaching cannot be applied. As such, it is not used in this study as an indication of trace element leaching, but only is compared to the Ba/Sr values reported by Retallack et al. (2003) in their paleosol classification scheme.

Comparison of Proxy Trends Across Karoo Studies

Paleoclimatic Proxies- Scheffler et al. (2003) concluded that proxy signals in the Karoo Basin indicate a climate that was warming and humid, but increasingly arid, during the Early Permian following Gondwanan deglaciation. This is largely based on CIA-K values which increase steadily above the Dwyka Group (median CIA-K of 55) and then decrease in the Middle Permian Ecca Group (median CIA-K of 80) as a drier climate impeded weathering (Scheffler et al., 2006). This large increase is attributed not only to climate warming, but also to the associated spread of land plants across the basin which intensified the weathering process (Scheffler et al., 2006). Subsequently, in the Middle-Late Permian Beaufort group, CIA-K values were reported to decrease as climate became increasingly arid (Scheffler et al., 2006). CIA-K values given by Scheffler et al. (2006) for the Beaufort Group plot in the 65 to 70 range, whereas the CIA-K values found in this study for the same stratigraphic interval have an average value of 80. There is a single outlier plotted by Scheffler et al. (2006) for the Ecca Group that has a significantly

higher value than all other siltstone intervals sampled by them. This sample was derived from a wetland paleosol and has CIA-K value of ~84 (Scheffler et al., 2006). The difference in overall CIA-K values reported for the Beaufort Group by Scheffler et al. (2006) and those reported in this study can be resolved by the fact that the NWP paleosol is a wetland paleosol, and thus would yield a higher weathering ratio. This illustrates that it is important to understand the type of interval sampled and to consider the environment of deposition during analysis and interpretation of paleoclimate.

Retallack et al. (2003) plot several soil molecular weathering ratios for a ~70 cm Bada paleosol profile. The method of calculation (use of wt.% oxide or molar abundance) are reported for how these profiles were constructed. Values range from ~0.05 to ~0.15 for clayeyness and ~0.5 to ~1 for calcification (Retallack et al., 2003). CIA values range from ~1 to ~2 (Retallack et al., 2003), which is impossibly low. Retallack et al. (2003) also report Ba/Sr values over ~70 cm profile depth for Late Permian Bada paleosols. These values all are at or below ~2 and are relatively constant, with a small overall decrease from ~2 to ~0.5 down-profile. The Ba/Sr plots for the NWP and OWP profiles have a total range of 2.06 to 8.12, and exhibit comparatively wide fluctuations within the paleosol. NWP Ba/Sr ranges from 2.32 to 8.12, OWP1 from 2.06 to 4.91, and OWP2 from 4.26 to 7.24, all of which are significantly higher values than those reported by Retallack et al. (2003). The higher overall Ba/Sr values indicate a greater degree of weathering in the Wapadsberg Pass paleosol than for Bada paleosols, which is the closest analogue in the Retallack et al. (2003) classification scheme. The soil molecular weathering ratios and Ba/Sr profiles in this scheme all exhibit an extremely small range in variation, and are constant within the paleosol profile compared with the patterns observed for the Wapadsberg Pass paleosol.

Geochemical Trends- Recently, Coney et al. (2007) published geochemical data from the Permian and Triassic of the Beaufort Group and Katberg Fm. at Wapadsberg Pass. Major- and trace-element abundances from ICP-OES analysis (Table 4) and XRF analysis (Table 5) are compared to element data reported by Coney et al. (2007) for Wapadsberg Pass (Table 8). The lowest stratigraphic interval analyzed by Coney et al. (2007) sits ~6 m below the PTB, whereas the Wapadsberg Pass paleosol sits ~70 m below the PTB. Thus, a contemporaneous

comparison is not possible. Comparing these data does allow for an idea of the geochemical trends while approaching the PTB, and the geochemistry of the paleosol relative to the surrounding rock. All major elements are common between this study and Coney et al. (2007), and common trace elements are Ba, Co, Cr, Cs, Cu, Ni, Sr, V, Zn, Eu, Gd, La, Nd, Sm, Yb and Y (Table 8). Trace element results from this study can be compared to those from Coney et al. (2007) to determine the geochemical trends that exist through time at this locality.

Elements that are known as plant toxins or that are potentially detrimental to plant growth in over-or-under abundances may provide insight into the nutrient quality of the Wapdsberg Pass soil. Toxic elements that typically inhibit plant growth in high concentrations include Fe, Mn, Zn, Ni, Cu, Ba, and Cr (Hunt, 1972). However, Mn, Zn, and Cu also may limit growth if soil concentrations are too low (Hunt, 1972). Limiting elements for plant-growth include Ca, Mg, and K, and leaching of these results in decreased soil fertility (Hunt, 1972).

The Wapadsberg Pass paleosol, relative to geochemical data from Coney et al. (2007), exhibits potentially stressed nutrient conditions. Fe, Ba, Cu, Cr, and Zn all are in high concentrations, and Ni is slightly high, when compared to other Wapadsberg Pass concentrations of these elements (Table 8). Common abundances of these elements in modern soils are on the order of 1 wt% for Mn, 10 ppm for Zn, 100 ppm for Cu and Ni, 1 ppm for Ba, and Cr in any small quantities is considered toxic (Hunt, 1972). The elemental abundances in this paleosol all conform to these magnitudes, except for Ba and Cu which both are anomalousy high (Table 8). The concentration of Ba ranges between 100-1000 ppm, and Cu is at 10 ppm. Elevated amounts of Cu are mildly toxic, and Ba causes a decreased yield in plants by shutting down their stomatal openings (Hunt, 1972). A Ba concentration this high would undoubtedly have affected the growth of *Glossopteris* in this soil.

There is an observed decrease in *Glossopteris*-leaf size from the Middle Permian into the latest Permian (Prevec et al., in press). *Glossopteris* leaves preserved in the forest-floor litter at NWP are small in relation to the size of the *Vertebraria*-root structures found at the same locality (Gastaldo, R.A., pers. communic., 2010). Leaves are 50-120 mm long and 4-23 mm wide,

A.

Major Elements	(wt %)							
sample interval	Al (Al2O3)	Ca (CaO)	Fe (Fe2O3)	K (K2O)	Mg (MgO)	Mn (MnO)	Na (Na2O)	Si (SiO2)
Coney, Wap. Pass (-0m)	9.45	21.4	3.23	2.06	1.43	1.5	0.83	38.6
Coney, Wap. Pass (-6m)	14.4	1.21	3.63	1.99	1.13	0.06	3.02	70.45
Knight (-70 m)(XRF)	17.86	1.28	5.31	3.96	1.76	0.09	1.30	67.31
expected concentrations						~1%		

B.

Trace Elements	(ppm)															
sample interval	Ba	Co	Cr	Cs	Cu	Ni	Sr	V	Zn	Eu	Gd	La	Nd	Sm	Yb	Y
Coney, Wap. Pass (-0m)	299	8	28	6.34	12	13	291	49	65	1.01	4.3	38.1	33	5.71	2.68	30
Coney, Wap. Pass (-6m)	3513	9	40	3.01	14	15	664	64	69	1.29	6.88	38.4	37.5	6.48	2.6	29
Knight (-70 m)(XRF)	821.77		63.85				186.77		92.77							
Knight (-70m)(ICP)																
av. NWP	741.9	17.8	51.8	742.2	19.8	27.1	168.0	94.6	98.9	0.4	14.6	36.0	150.4	9.6	1.9	25.1
av. OWP1	658.7	9.6	69.0	659.1	15.9	15.9	230.7	76.4	76.2	0.4	11.1	26.1	124.2	8.4	1.4	19.5
av. OWP2	794.6	10.5	50.6	795.0	18.6	14.7	140.5	100.9	81.0	0.3	13.5	27.1	129.0	9.2	1.4	19.0
av. (total)	736.1	13.6	55.8	736.5	18.5	20.8	175.8	91.8	88.1	0.4	13.4	31.0	137.7	9.2	1.6	22.0
expected concentrations	~1 ppm	~100 ppm	~10 ppm		~100 ppm	~100 ppm	~10 ppm	~10 ppm	~10 ppm			~100 ppm				~100 ppm

Table 8 – Comparison of major and trace element geochemical data (XRF and ICP-OES) from this study to Coney et al. (2007), for all Wapadsberg Pass localities (NWP, OWP1, and OWP2). A.- Major elements. B.- Trace elements

compared to roots up to 2 cm in diameter that imply meter-scale trees (Prevec et al., in press). They speculated that this apparent stunted growth could be an artifact of soil toxicity, and one aim of the present geochemical analysis of the Wapadsberg Pass paleosol was to investigate this possibility. The results show elevated concentrations of plant toxins, especially Ba and Cu, leading to the conclusion that soil conditions at Wapadsberg Pass were poor and may have induced stunted growth of *Glossopteris*. However, better resolution of the spatial and temporal geochemical trends in the Karoo Basin is needed to substantiate this conclusion.

Paleoenvironmental Interpretations

The paleosol at Wapadsberg Pass formed on an aggradational floodplain, proximal to a fluvial channel. The water table would have been high enough to create wetland conditions, inhabited by a *Glossopteris* forest with a sphenopsid understory of *Trizygia* and *Phyllotheca*. Climate during the Late Permain is interpreted to have undergone significant seasonal fluctuation, based on the nature of the fluvial channels (Ward et al., 2000) and the stratigraphy. Cyclic changes within fluvial depositional systems such as those observed at Wapadsberg Pass are likely to be related to short-term changes in climate (Sheldon and Tabor, 2009), and may reflect strong seasonality in the Late Permian.

The 13 cm thick claystone that caps the NWP paleosol is not an air fall deposit, based on the orientation of the preserved flora, which lay flat. Fine laminations are present and the ash sequence resembles a lake-deposit, leading to the interpretation that it was fluvially deposited. Laminated ash with preserved organic matter is found at 0 cm, -8 cm, and -20 cm depth, in addition to several other intervals within the NWP stratigraphic section (at 601 cm and 700 cm (Fig. 3)). Ash balls, interpreted to be re-worked and fluvially deposited based on their well-rounded appearance, are found at -30 cm within the soil profile. This abundance of river-deposited ash requires some mechanism by which the sediment load in the fluvial channel becomes composed almost entirely of ash or large (cm-scale) reworked ash clasts during repeated episodes of flooding. The sediment load must have consisted overwhelmingly of tuffite to generate the nearly pure ash deposits and the intermixed ash balls across the floodplain as it was inundated. One possible scenario that would explain the ash deposit-types at NWP is the

repeated damming, and then releasing, of the channel by volcanogenic material (Gastaldo, pers. communic., 2010). The number of tuffite deposits observed in the NWP stratigraphic section suggests frequent and abundant volcanic activity over the period during which this sequence was deposited, and the influx of volcanogenic material into the fluvial system may have blocked river flow with accumulated tuffite. In this scenario, the ash deposits represent the failing and washing out of these dams. A failed tuffite dam could simultaneously overwhelm the fluvial-sediment load with either unconsolidated or partially lithified tuffite and induce an episode of flooding. The unconsolidated ash would be deposited as the laminite sequences observed at 0 cm, -8 cm, and -20 cm depth, and partially lithified tuffite would be re-worked by the stream and deposited as the well-rounded ash-balls observed at -30 cm depth in the NWP paleosol.

Sheldon and Tabor (2009) provide equations for calculating MAT (mean annual temperature) (specific to inceptisols) and MAP (mean annual precipitation). The MAT equation is T(˚C)=4.69c+4, where c is the clayeyness value of the Bt (clay) horizon, and standard error is ±0.6˚C. The MAP equation is P(mm/yr)=221.1e^(0.0197(CIA-K)), where the CIA-K value of the Bt horizon is used, and the standard error is ±181 mm/yr. While there is no well-developed Bt horizon in the Wapadsberg Pass paleosol, there are slight excursions in clayeyness and CIA-K observed at -25 cm depth which will be used as the Bt horizon for the purposes of calculating MAT and MAP. These calculations yielded a temperature of 12.24˚C and 1200.21 mm of precipitation per year, measures that support the interpretation of a seasonal climate. The MAT is lower than might be expected given the reported trend of warming through the Middle into the Late Permian (Scheffler et al., 2006). However, it is important to consider the seasonal aspect of this result. Seasonal climates typically have large daily and seasonal temperature fluctuations. These temperature changes also may be responsible for having induced a stress response in *Glossopteris*. Hence, the small size of the NWP leaves may not have been in response to warming of the climate, as suggested by Smith (1995), Ward et al. (2000), and Retallack et al. (2003), but to cooling. If *Glossopteris* were cold-intolerant and subjected to nightly and seasonal intervals of low temperatures, these conditions may have been another mechanism responsible for the stunting of their growth. If the presence of abundant volcanism evidenced in the

stratigraphic record at Wapadsberg Pass is considered further, it is possible that the low MAT may also be the result of volcanic ash input into the atmosphere. This would cause a regional and temporally brief drop in temperature as the sun was blocked by ash particles in the atmosphere. These estimates of MAT and MAP may not be the most reliable due to the lack of a well-defined Bt horizon in the NWP paleosol, but they allow a general quantification of paleoclimatic conditions.

Conclusions

The Karoo Basin, South Africa, has been the focus of numerous studies investigating the Permian-Triassic mass extinction event in an attempt to constrain the timing and placement of the PTB. However, few studies have concentrated on the use of paleosols and their associated geochemistry in this region as measures of paleoenvironmental factors. This study is the first to perform a high-resolution analysis of a Late Permian paleosol within stratigraphic context and geochemical trends within its profile. This paleosol and associated well-preserved forest-floor leaf-litter was reported by Reid et al. (2007) to crop out in New and Old Wapadsberg Pass (S 31° 55.927', E 24° 52.872', and S 31° 55.199', E 24° 53.666' and S 31° 55.108', E 24° 53.692', respectively) along a single isochronous horizon ~70 m below the vertebrate-defined PTB. The floral assemblage represents a forest canopy of the gymnosperm tree *Glossopteris* and an understory of the sphenopsids *Phyllotheca* and *Trizygia* (Prevec et al., in press). This paleosol is unique to the basin in that it includes a well-preserved forest-floor litter as an O-horizon, does not fit any of the previously defined Karoo soil classification schemes (Smith, 1995; Retallack, 2003; Smith and Botha, 2005; Botha and Smith, 2006), and exhibits volcanic influence in the form of ash and intermixed tuffite.

To classify the Wapadsberg Pass paleosol and describe its stratigraphic context, several types of analyses were performed. These included the construction of a high-resolution (cm-scale) stratigraphic column for the NWP and OWP sections, examination of petrographic thin sections taken from the paleosol profile, and interpretation of the geochemical data and proxy trends. Based on the integrated results of these analyses, it was concluded that the Wapadsberg

Pass paleosol profile represents a stacked inceptisol, deposited in an aggradational floodplain setting with a high water table, and colonized by *Glossopteris*-dominant forest. The stratigraphy of the paleosol is such that each of the two interpreted soil surfaces, at 0 cm and -25 cm profile depth, is overlain by a tuffite deposit and corresponds to an underlying TOC spike interpreted to represent the soil's O-horizon. Petrographic thin sections also revealed angular-to-rounded quartz grains within the paleosol, concentrated at -30 and -60 cm profile depth, interpreted to be intermixed tuffite. The horizons of tuffite, and the rounded ash balls (~10 cm diameter) concentrated at -30 cm depth, support the interpretation that the NWP profile contains a stacked paleosol. The limited depth between the older and younger paleosol surfaces indicates a shallow water table was present at the time of soil formation, and reflects a wetland environment. TOC:TON is consistently less than 10, exhibiting what is considered to be an algal signature (Scheffler et al., 2003). However, the samples analyzed are of a terrestrial paleosol within a fluvial sequence, and one possible explanation for the low ratio values is the abundance of freshwater algae in this wetland setting. The presence of leaves from *Glossopteris*, a wetland plant, in the forest-floor assemblage supports the conclusion that the water table was locally high.

A shift in climate from warm and humid, to warmer and more arid is reported for the Middle-Late Permian (Scheffler et al., 2003; 2006). The paleosol resides under these transitional environmental conditions and reflects climate variation during this time. Based on analyses of the Wapadsberg Pass paleosol and surrounding stratigraphy, climate during the Late Permian is interpreted to have been highly seasonal, fluctuating between wet and dry periods. Carbonate nodules in soils below the NWP paleosol are reported to have a wet-environment signature (based on carbon isotopic studies (Tabor et al., 2007)), while nodules at the contact between laminated siltstone and overlying sandstone above it exhibit a dry seasonal signature (Reid et al., 2007). These are evidence of seasonality on a local scale at this locality. The cyclic nature of the aggradational and degradational fluvial deposits at Wapadsberg Pass also supports short-term climatic variation (Sheldon and Tabor, 2009), with aggradation occurring during the wet season.

Approaching the PTB, there is a decrease in Glossopteris leaf size observed through time (Prevec et al., in press), and one aim of this study was to investigate the element-toxicity in

soils as a potential mechanism to explain this trend. Compared to other geochemical data for Wapadsberg Pass (Coney et al., 2007), the NWP paleosol exhibits extremely high concentrations of Ba, and elevated concentrations of Fe, Cu, Cr, and Zn. The high concentrations of these elements, known to be toxic to plants, are likely to have had some degree of detrimental effect on the productivity and growth of *Glossopteris* colonizing this soil.

The examination of the Wapadsberg Pass paleosol has aided in constraining the paleoenvironmental conditions present during the latest Permian of the Karoo Basin. However, this study is by no means comprehensive, as it represents only a (geologically) single point in time and space in the Karoo Basin. Further high-resolution description of paleosols and additional geochemical work is needed to better constrain paleoclimatic trends leading up to the PTB. Paleosols provide a variety of petrographical and geochemical tools that allow direct interpretation of paleoclimate and paleoenvironment. The application of these tools to Karoo Basin paleosols across spatial and temporal frames could provide the best-resolution for the description of these trends for the Middle Permian through the Early Triassic. This would aid in resolving some of the uncertainty surrounding the conditions present at the PTB and the terrestrial response, if any, to the Permain-Triassic mass extinction event.

Personal Communications

Gastaldo, Robert A. Department of Geology, Colby College, 5800 Mayflower Hill Drive, Waterville, ME 04901. ragastal@colby.edu

Prevec, Rose C. Department of Geology, Rhodes University, P.O. Box 94, Grahamstown, 6410, South Africa.

Neveling, Johann. Council for Geosciences, Private Bag x112, Pretoria, 0001, South Africa.

Tabor, Neil J. Department of Geological Sciences, Southern Methodist University, P.O. Box 750395, Dallas, TX 75275-0395

Crapster-Pregont, E. Colby College. ejcrapst@colby.edu

Pludow, Amelia. Colby College. bapludow@colby.edu

References

Botha, J., and Smith, R.M.H., 2006, Rapid vertebrate recuperation in the Karoo Basin of South Africa following the End-Permian extinction: Journal of African Earth Science, v. 45, p. 502-514.

Catuneanu, O., Hancox, P.J. and Rubidge, B.S. (1998). Reciprocal flexural behaviour and contrasting stratigraphies: A new basin development model for the Karoo retroarc foreland system, South Africa. Basin Research, 10, 417-439.

Coney, L., Reimold, W.U., Hancox, J.P., Mader, D., Koeberl, C., McDonald, I., Stuck, U., Vajda, V., and Kamo, S.L., 2007, Geochemical and mineralogical invstigation of the Permian-Triassic boundary in the continental realm of the southern Karoo Basin, South Africa: Paleoworld, v. 16, p. 67-104.

DeKock, M.O., and Kirschvink, J.L., 2004, Paleomagnetic Constraints on the Permian-Triassic Boundary in Terrestrial Strata of the Karoo Supergroup, South Africa: Implications for Causes of the End-Permian Extinction Event: Gondwana Research, v. 7, p. 175-183.

Douchafour, P., 1977, Pedology: Pedogenesis and classification. English edition translated by George Allen and Unwin. George Allen & Unwin Publishers Limited.

Gastaldo, R.A., Adendorff, R., Bamford, M, Labandeira, C.C., Neveling, J, and Sims, H., 2005, Taphonomic trends of macrofloral assemblages across the Permian-Triassic boundary, Karoo Basin, South Africa: Palaios, v. 20, p. 480-498.

Gastaldo, R.A., Neveling, J., Clark, K.C., and Newbury, S.S., 2009, The terrestrial Permian-Triassic boundary event bed is a non-event: Geology, v. 37, p. 199-202.

Gastaldo, R.A., and Rolerson, M.W., 2008, Katbergia gen. nov., a new trace fossil from the Late Permian and Early Triassic of the Karoo Basin: Implications for paleoenvironmental conditions at the P/Tr extinction event: Palaeoecology, v. 51, p. 215-229.

E.S. Gladney, E.S., and Roelandts, I., 1988, 1987 Compilation of Elemental Concentration Data for USGS BIR-1, DNC-1 and W-2: Geostandard Newsletters, v. 12, p. 63.

Johnson,M.R., van Vuuren, C.J., Visser, J.N.J., Cole, D.I., Wickens, H.deV., Christie, A.D.M., Roberts, D.L., and Brandl, G., 2006, Sedimentary rocks of the Karoo Supergroup: Geology of South Africa, v. 22, p. 461-495.

Hunt, C.B., 1972, Geology of Soils: Their Evolution, Classification, and Uses. W.H. Freeman and Company.

Lahann, R.W., 1980, Smectite Diagenesis and Sandstone Cement: The Effect of Reaction Temperature: Journal of Sedimentary Research, v. 50.

MacLeod, K.G., Smith, R.M.H., Koch, P.L., and Ward, P.D., 2000, Timing in mammal-like reptile extinctions across the Permian-Triassic boundary in South Africa: Geology, v. 28, p. 227-230.

Mundil, R., Ludwig, K.R., Metcalfe, I., Renne, P.R., 2004, Age and Timing of the Permian Mass Extinctions: U/Pb Dating of Closed-System Zircons: Science, v.305, p. 1760-1763.

Pace, D.W., Gastaldo, R.A., and Neveling, J., 2009, Early Triassic aggradational and degradational landscapes of the Karoo Basin and evidence for climate oscillation following the P-Tr event: Journal of Sedimentary Research, v. 79.

Prevec, R., Gastaldo, R.A., Neveling, J., Reid, S.B., Looy, C.V., in press, An autochthonous glossopterid flora with Latest Permian palynomorphs from the *Dicynodon* Assemblage Zone of the southern Karoo Basin, South Africa.

Pollastro, R.M., 1982, A recommended procedure for the preparation of oriented clay-mineral

specimens for X-ray diffraction analysis: Modifications to Drever's Filter Membrane peel technique: Open File Report 87-71.
Reid, S.B., Gastaldo, R.A., Neveling, J., and Prevec, R., 2006, Late Permian fluvial facies and architectures preserving an autochthonous leaf litter, Wapadsberg Pass, Eastern Cape Province, South Africa: Geological Society of America *Abstracts with Programs*, Vol. 38, No. 7, p. 144.
Reid, S.B., Gastaldo, R.A., Neveling, J., and Tabor, N.J., 2007, Fluvial systems and carbonate nodules reveal Late Permian climate change at Wapadsberg Pass, Eastern Cape Province, South Africa: Geological Society of America *Abstracts with Programs*, Vol. 39, No. 6, p. 85.
Retallack, G.J., 2001, Soils of the Past: An Introduction to Paleopedology. Second edition. Blackwell Science Limited.
Retallack, G.J., Smith, R.M.H., and Ward, P.D., 2003, Vertebrate extinction across Permian-Triassic boundary in Karoo Basin, South Africa: Geologocal Society of America, Bulletin, v. 115, pfd. 1133-1152.
Scheffler, K., Hoernes, S., Schwark, L., 2003, Global changes during Carboniferous-Permian glaciation of Gondwana: Linking polar and equatorial climate evolution by geochemical proxies: Geology, v. 31, p. 605-608.
Scheffler, K., Buehmann, D., Schwark, L., 2006 Analysis of late Palaeozoic glacial to postglacial sedimentary successions in South Africa by geochemical proxies – Response to climate evolution and sedimentary environment: Palaeogeography, Palaeoclimatology, Palaeoecology, v. 6, p. 184-203.
Sheldon, N.D., Retallack, G.J., and Tanaka, S., 2002, Geochemical climofluctuations from North American soils and application to paleosols across the Eocene-Oligocene boundary in Oregon: The Journal of Geology, v. 110, p. 687-696.
Sheldon, N.D., and Tabor, N.J., 2009, Quantitative paleoenvironmental and paleoclimatic reconstruction using paleosols: Earth Science Reviews, v. 95, p. 1-52.
Smith, R.M.H., 1995, Changing fluvial environments across the Permian-Triassic boundary in the Karoo Basin, South Africa, and possible causes of tetrapod extinctions: Palaeogeography, Palaeoclimatology, Palaeoecology, v. 117p. 81-104.
Smith, R.M.H., and Botha, J., 2005, The recovery of terrestrial vertebrate diversity in the South African Karoo Basin after the end-Permian Extinction: Compte Rendu Palevol, v. 4, p. 555-568.
Smith, R.M.H., Erickson, P.A., and Botha, W.J., 1993, A review of the stratigraphy and sedimentary environments of the Karoo-aged basins of Southern Africa: Journal of African Earth Sciences, v. 16, p. 143-169.
Smith, R.M.H., and Ward, P.D., 2001, Pattern of vertebrate extinctions across an event bed at the Permian-Triassic boundary in the Karoo Basin of South Africa: Geology, v.29, p.1147-1150.
Tabor, N.J., Montanez, I.P., Steiner, M.B., and Schwindt, D., 2007, $\delta^{13}C$ values of carbonate nodules across the Permian-Triassic boundary in the Karoo Supergroup (South Africa) reflect a stinking sulfurous swamp, not atmospheric CO2: Palaeogeography, Palaeoclimatology, Palaeoecology, v. 252, p. 370-381.
Ward, P.D., Botha, J., Buick, R., DeKock, M.O., Erwin, D.H., Garrison, G., Kirschvink, J., and Smith, R.M.H., 2005, Abrupt and gradual extinction among Late Permian land vertebrates in the Karoo Basin, South Africa: Science, v. 307, p. 709-714.
Ward, P.D., Montgomery, D.R., and Smith, R.M.H., 2000, Altered river morphology in South Africa related to the Permian-Triassic extinction: Science, v. 289, p. 1740-1743.

Figures

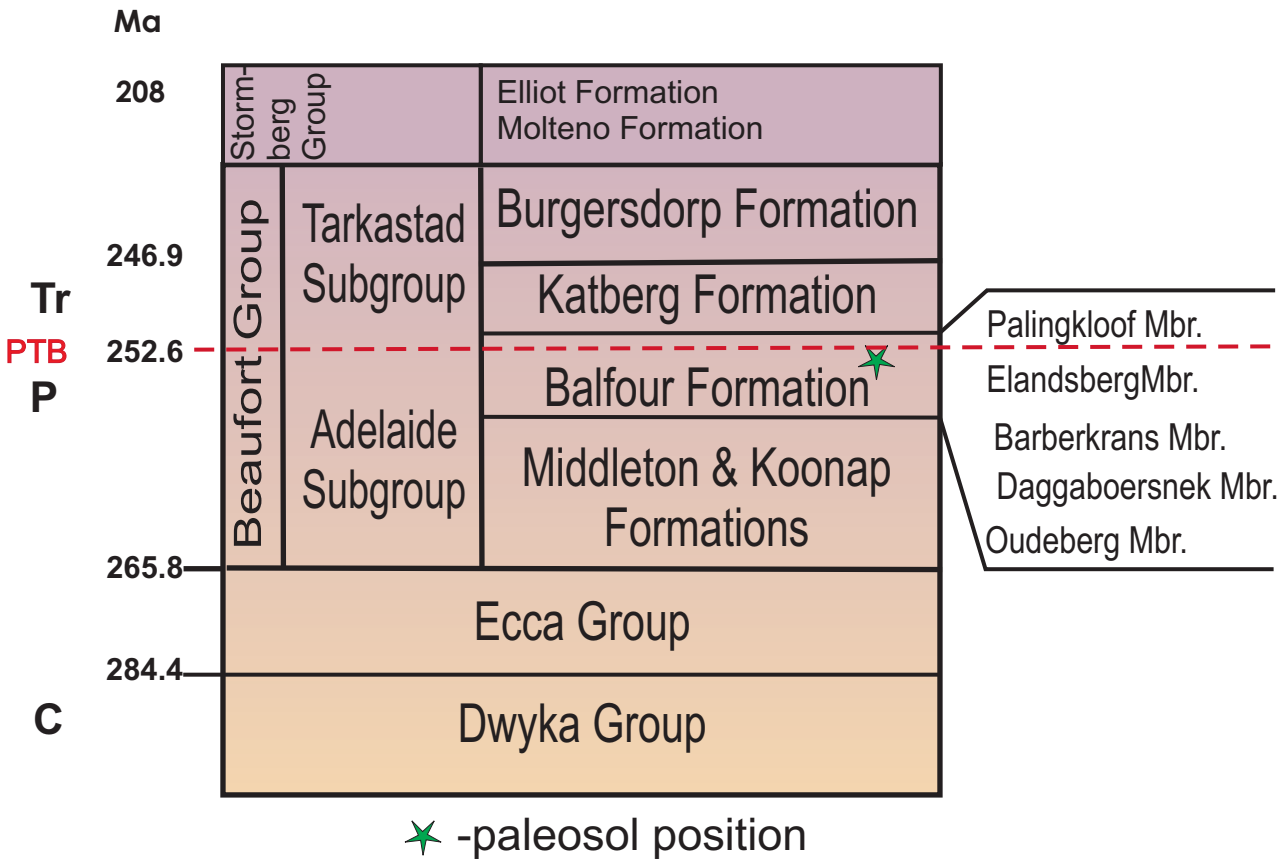

Fig. 1- General overview of the Karoo Supergroup stratigraphy. The PTB is placed at 252.6 ± 0.2 Ma (Mundil et al, 2004), as is defined by vertebrate biostratigraphy. The sratigraphic location of the Wapadsberg Pass paleosol is marked with a star, and is located between the Elandsberg and Palingkloof Members.

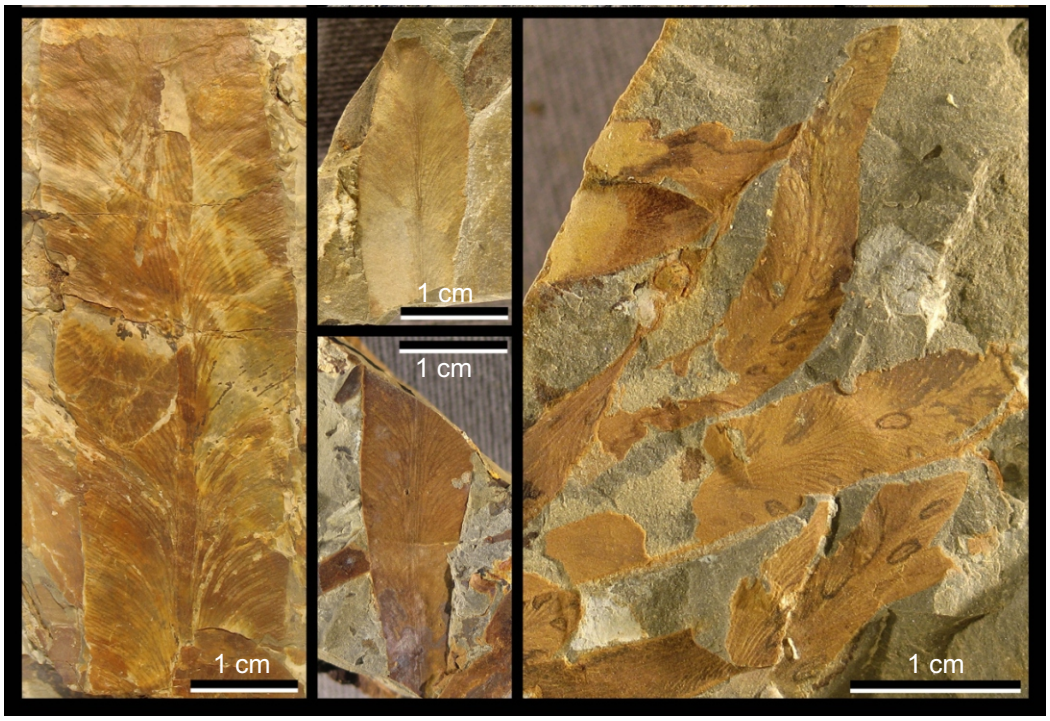

A

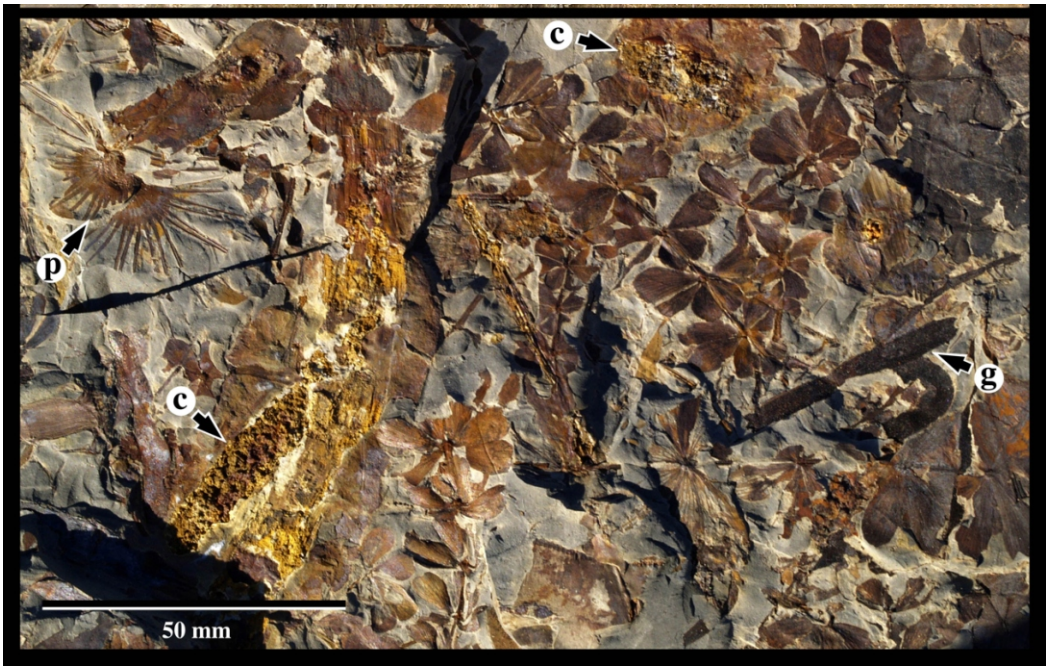

B

Fig. 2- Photographs of the forest-floor megaflora found in Wapadsberg Pass. A- *Glossopteris* leaves. B- The sphenopsid groundcover *Trizygia*. Letters indicate: p- *Phyllotheca*, c- sphenopsid cone, g- *Glossopteris*. (Prevec et al., in press)

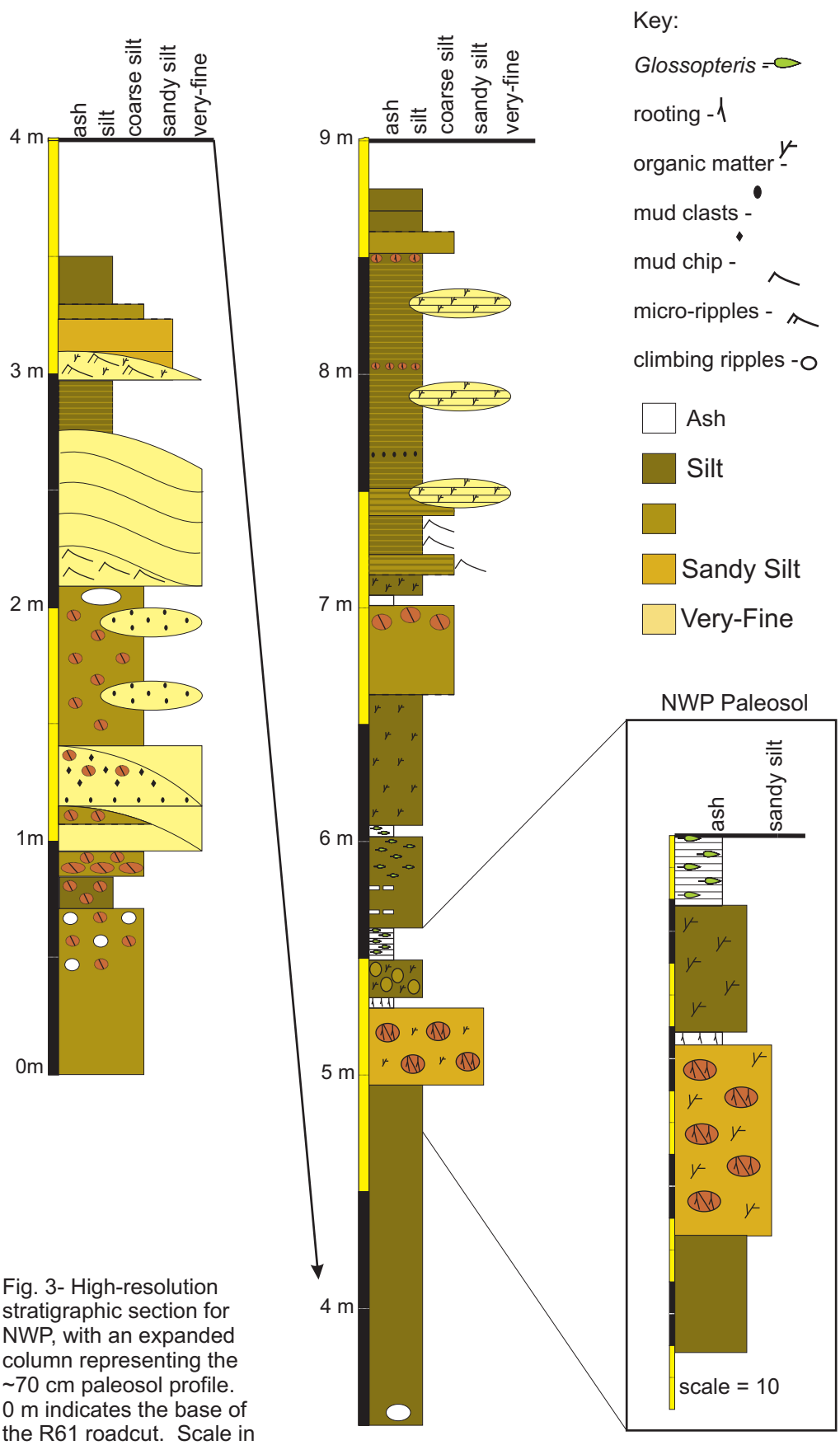

Fig. 3- High-resolution stratigraphic section for NWP, with an expanded column representing the ~70 cm paleosol profile. 0 m indicates the base of the R61 roadcut. Scale in

Fig. 4- Locality map for Wapadsberg Pass, Eastern Cape Province. The NWP outcrop along R61 and the OWP outcrops in dongas along the abandoned Wapadsberg Pass Road are marked by stars. NWP and OWP localities are isochronous outcrops of the paleosol. This study focuses on the NWP outcrop.

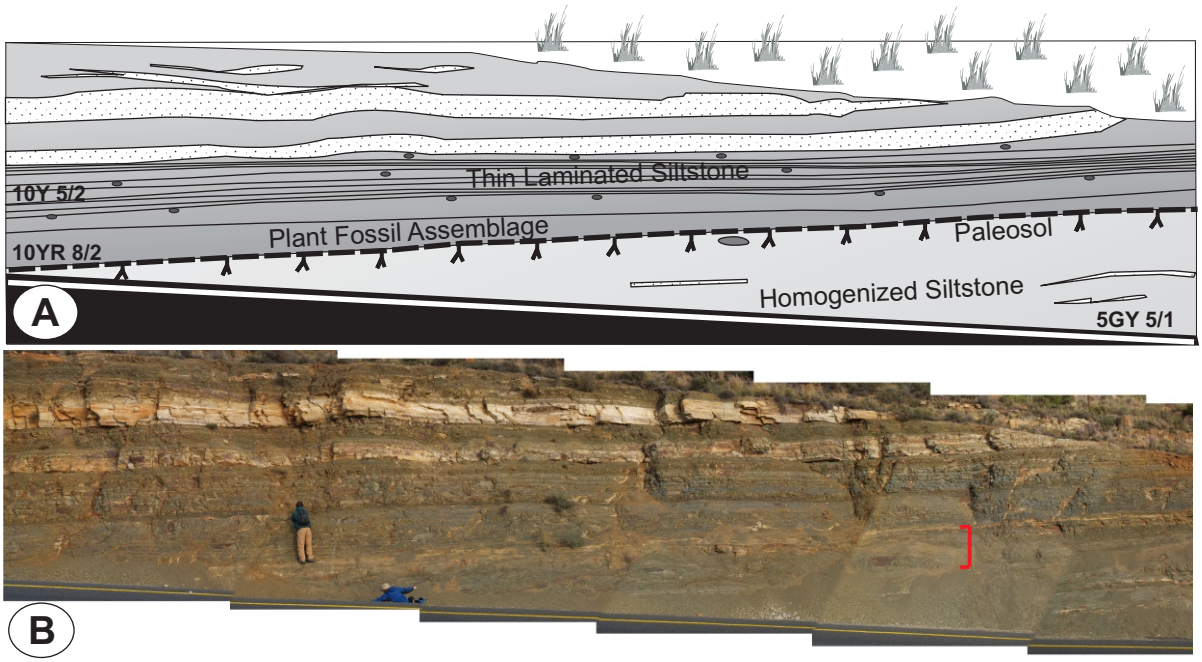

Fig. 5- The exposed stratigraphic section along R61 in which the NWP paleosol is found. A- a traced sequence identifying siltstone lithofacies, and the rooted NWP paleosol with associated fossil-plant bearing horizon. B- Photomosaic of the sequence in the R61 roadcut. NWP paleosol position (see Fig.3) is denoted by red brackets.

A

B

Fig. 6- Field photographs. A- the white claystone, interpreted to be an ash deposit, overlying the paleosol at NWP. B- a sampled paleosol profile at OWP. Scale in decimeters.

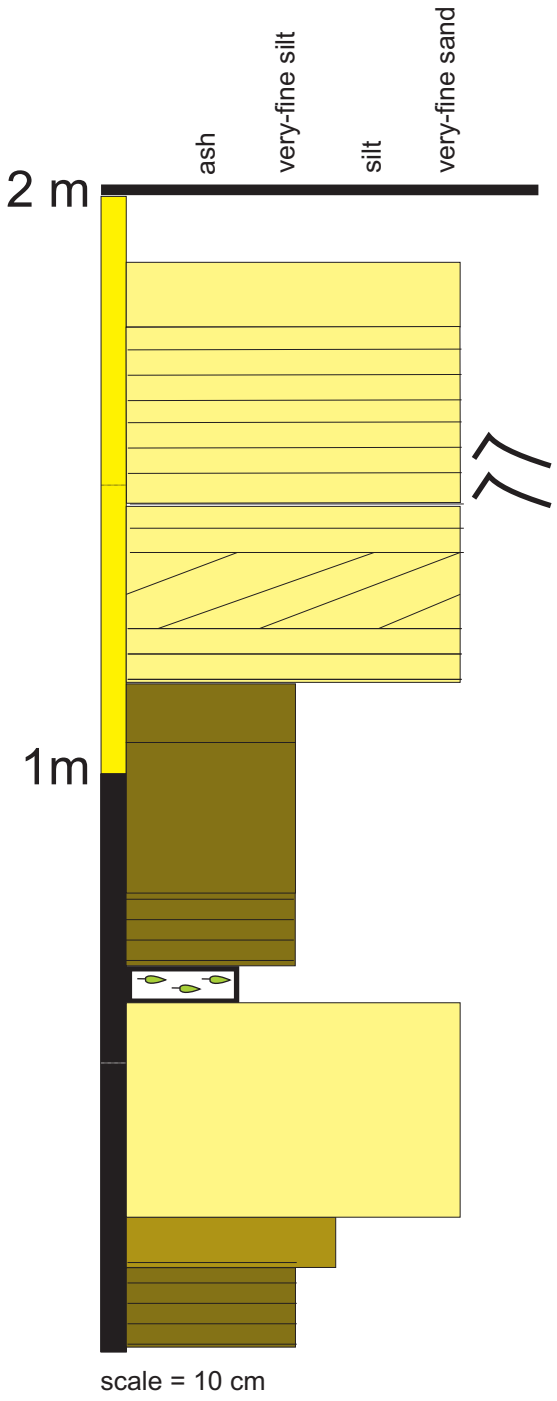

Fig. 7- High-resolution (cm-scale) stratigraphic column for OWP. The paleosol profile occurs between 0.7 m and 0 m in this section, capped by the ash deposit containing preserved *Glossopteris* leaves. Scale in meters.

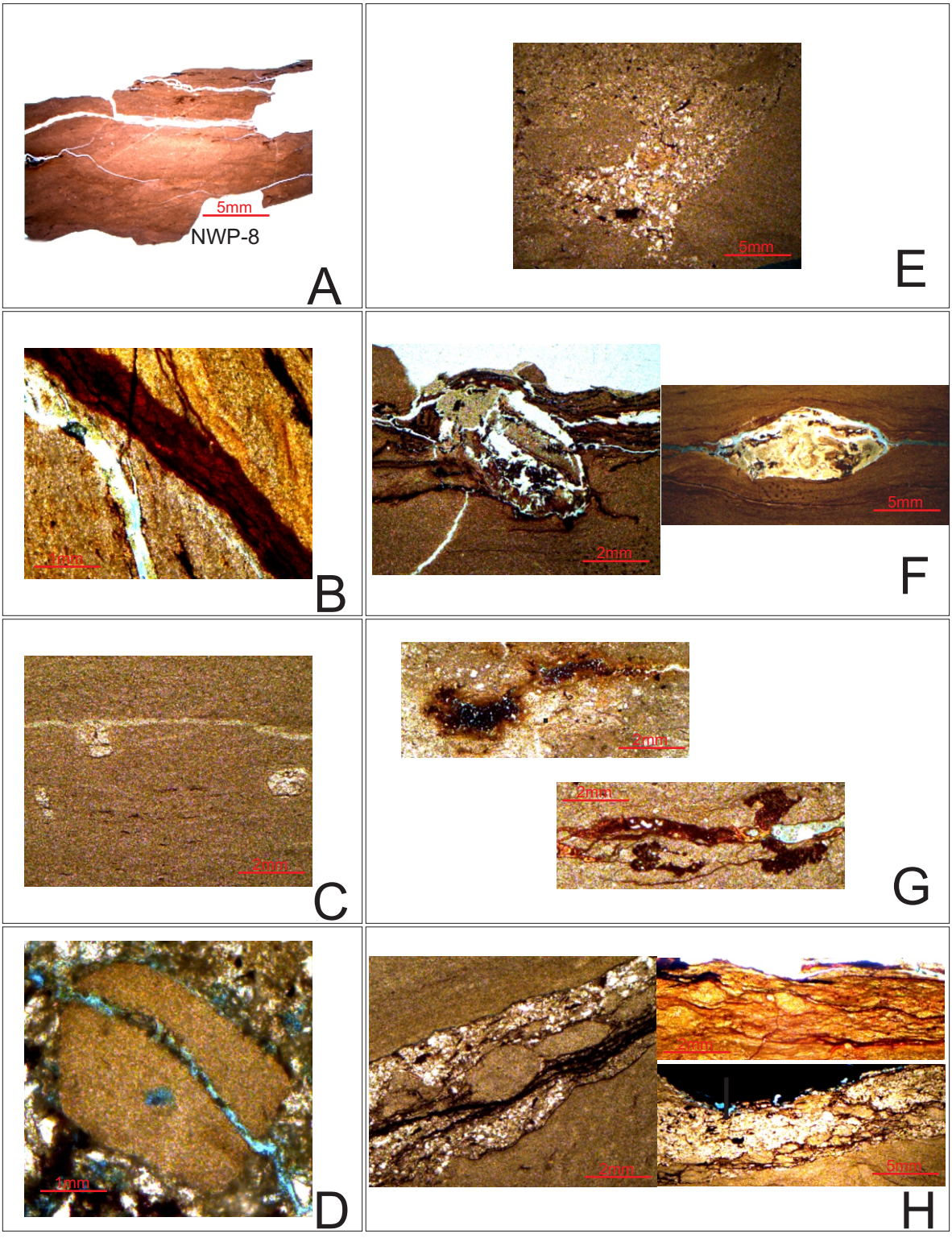

Figure 8 - Photographs of paleosol features visible in thin section. A- Concentrated OM, along the top of the section, at -8 cm depth in the NWP profile. B- Large, amber colored root (at OWPLH). C- Intermixed, singular round quartz grains (these from NWP-30). D- Yellowish, geometrically shaped clast present in the NWP and OWP profiles at -30 cm depth. E- Pocket of densely packed angular to rounded quartz grains intermixed in a fine silt matrix, at NWP-60. F- Rounded structures wrapped by bedding, associated with OM, and including the yellowish clasts observed at NWP-30 and possible interstitial mineral growth. These occur at OWP2-30. G- Pockets of spherical iron nodules, concentrated at -50 cm in the OWP profiles. H- Rooting structures with associated pockets of coarser material at -70 cm in the OWP profiles.

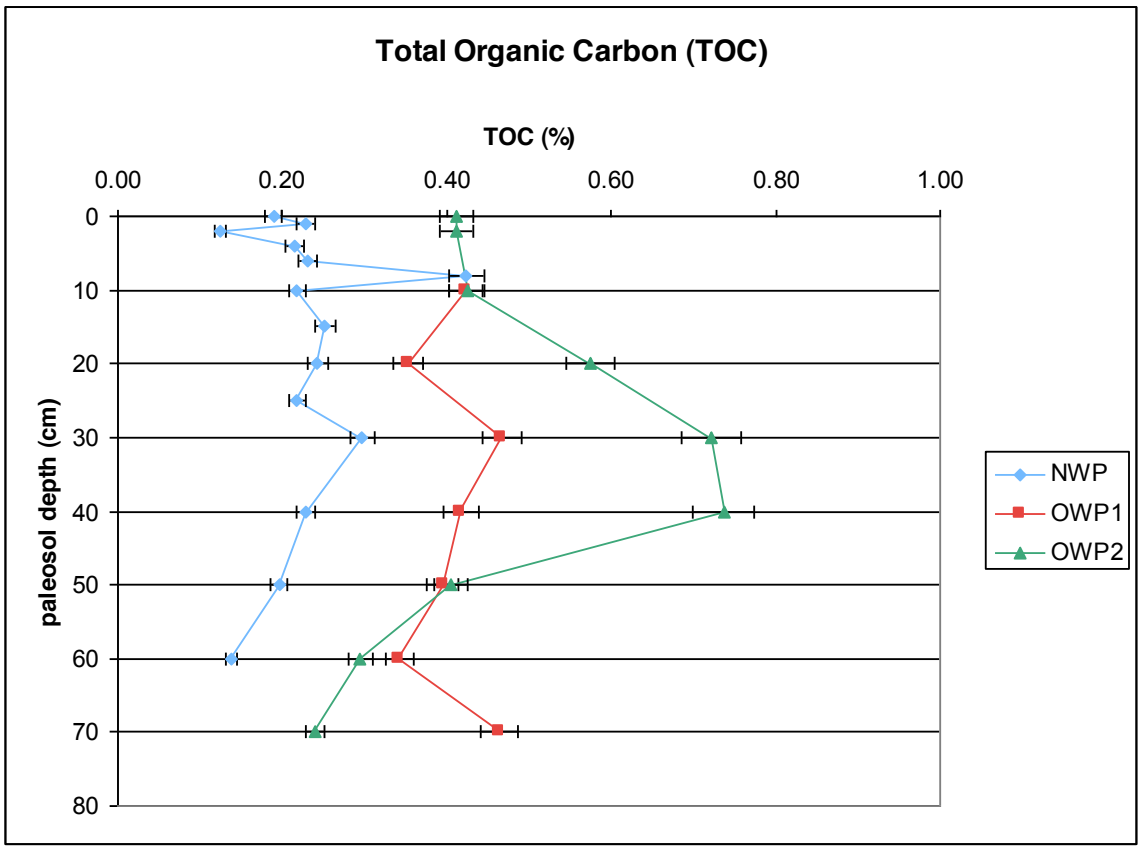

Fig. 9- Plot of TOC v. paleosol profile depth for NWP, OWP1, and OWP2 locations. Data from CHNO-S analysis are used. Error bars are 5%.

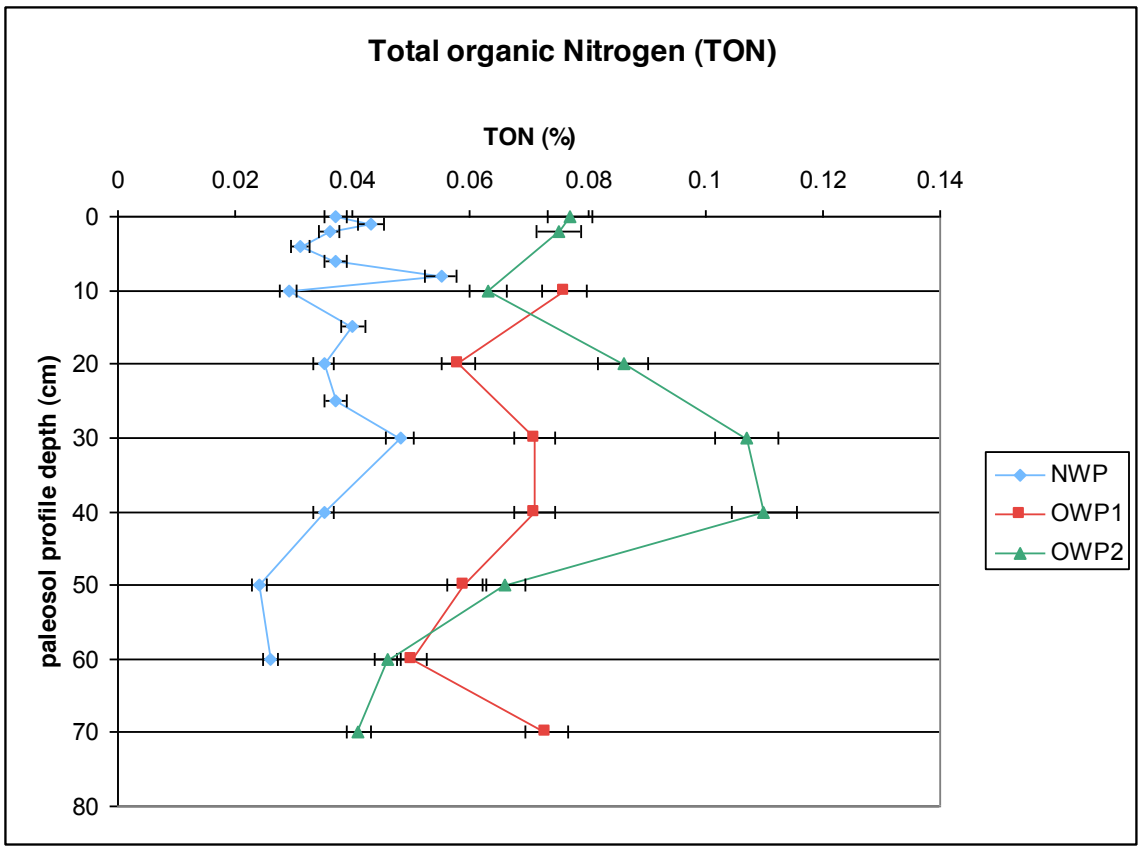

Figure 10- Plot of TON v. paleosol profile depth using CHNO-S data. Error bars are 5%.

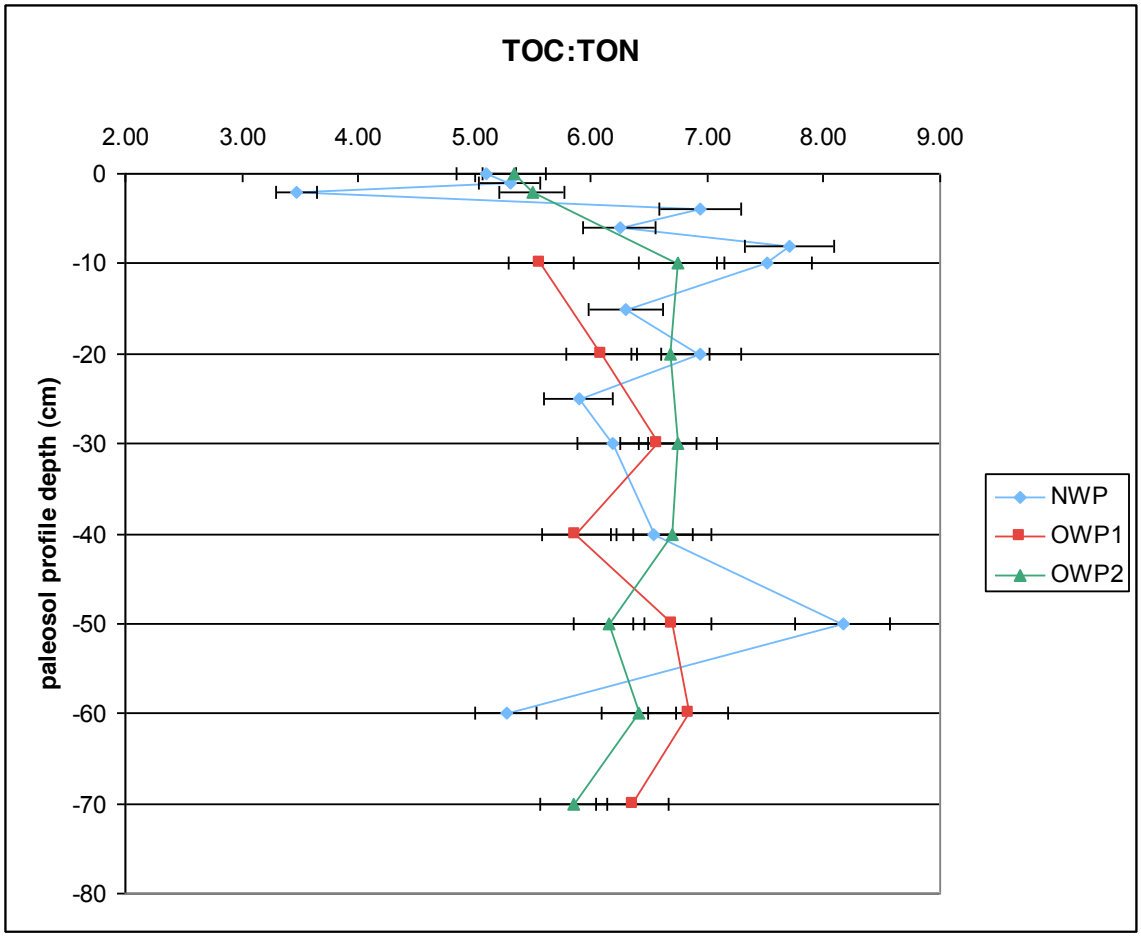

Fig. 11- Plot of TOC:TON values v. paleosol profile depth for NWP, OWP1, and OWP2 locations. Data from CHNO-S analysis are used. Error bars are 5%.

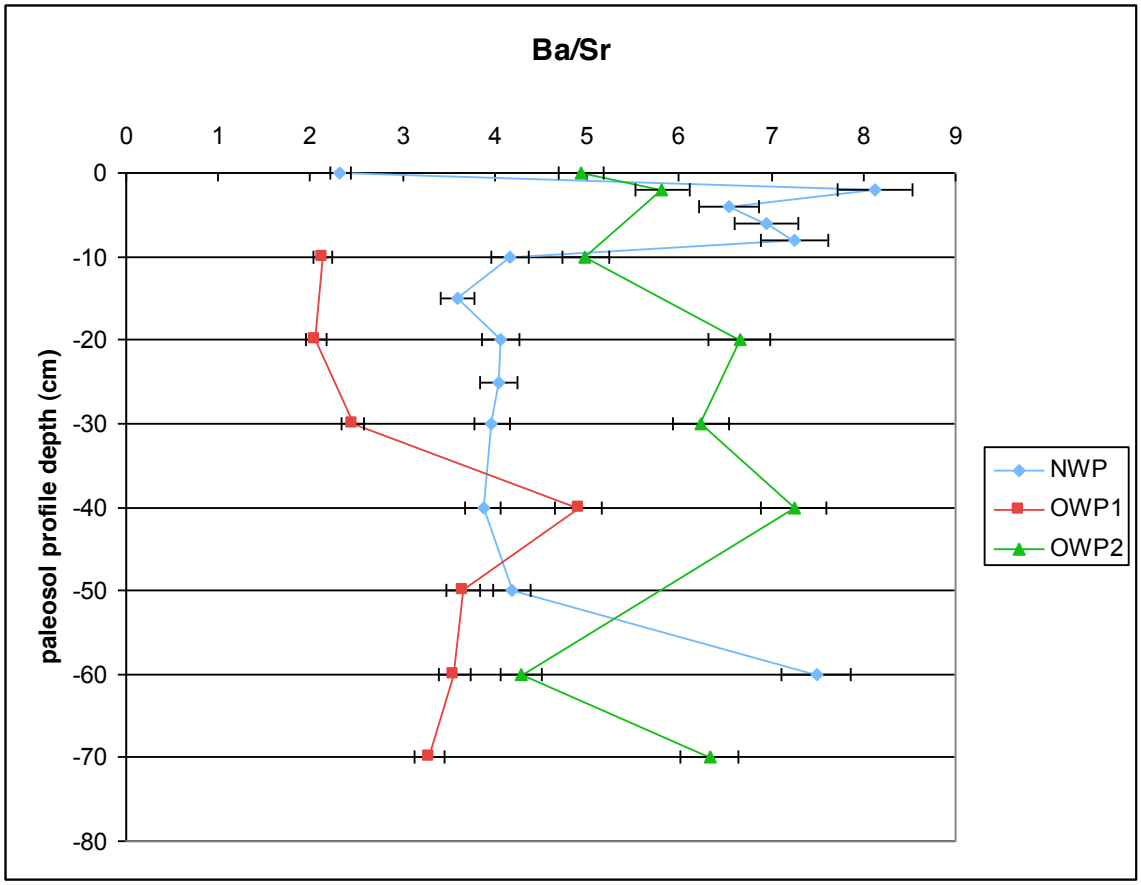

Fig. 12- Ba/Sr plotted v. paleosol profile depth for NWP. Trace element data from ICP-OES analysis are used. Ba/Sr is used as a proxy for leaching of trace elements, resulting from weathering intensity. Error bars are 5%.

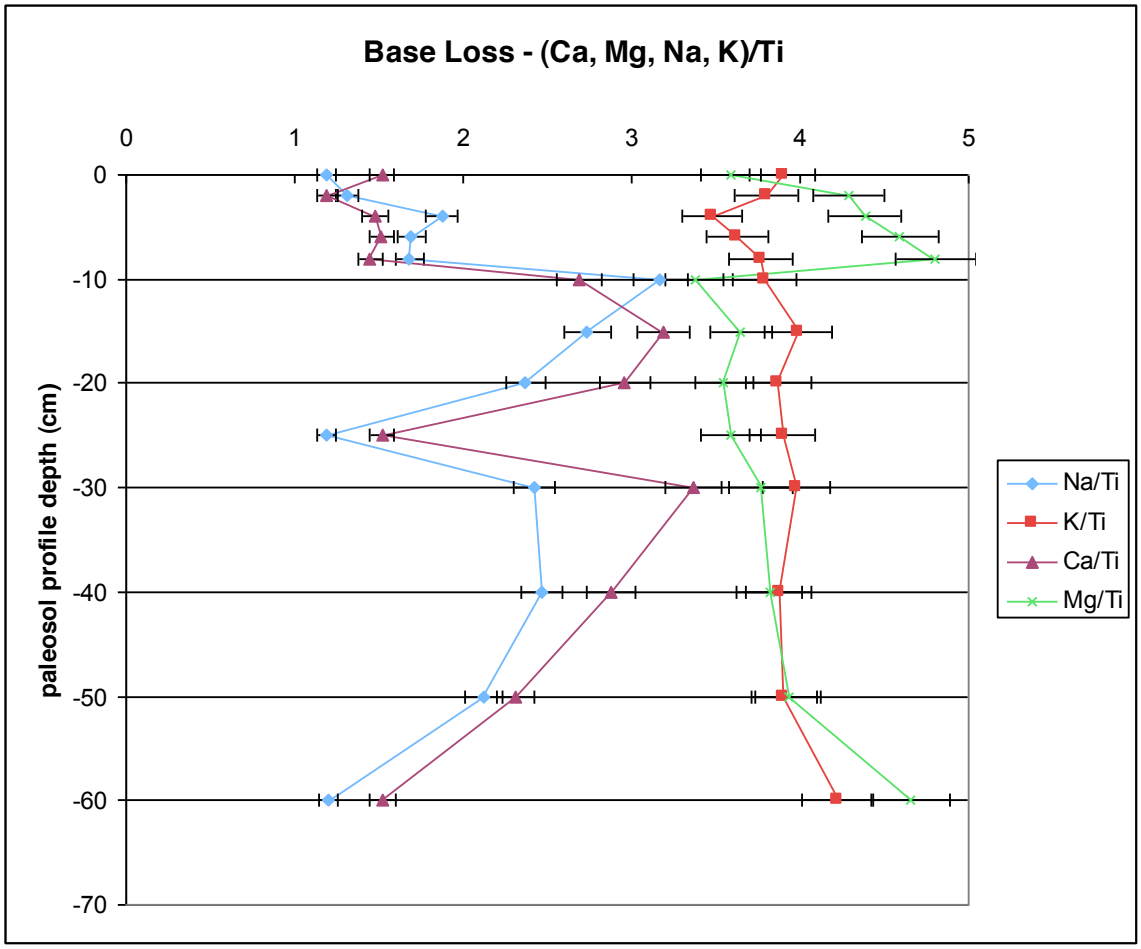

Fig. 13- Base loss calculated for Na, Ca, Mg, and K plotted v. paleosol profile depth for NWP. Error bars are 5%.

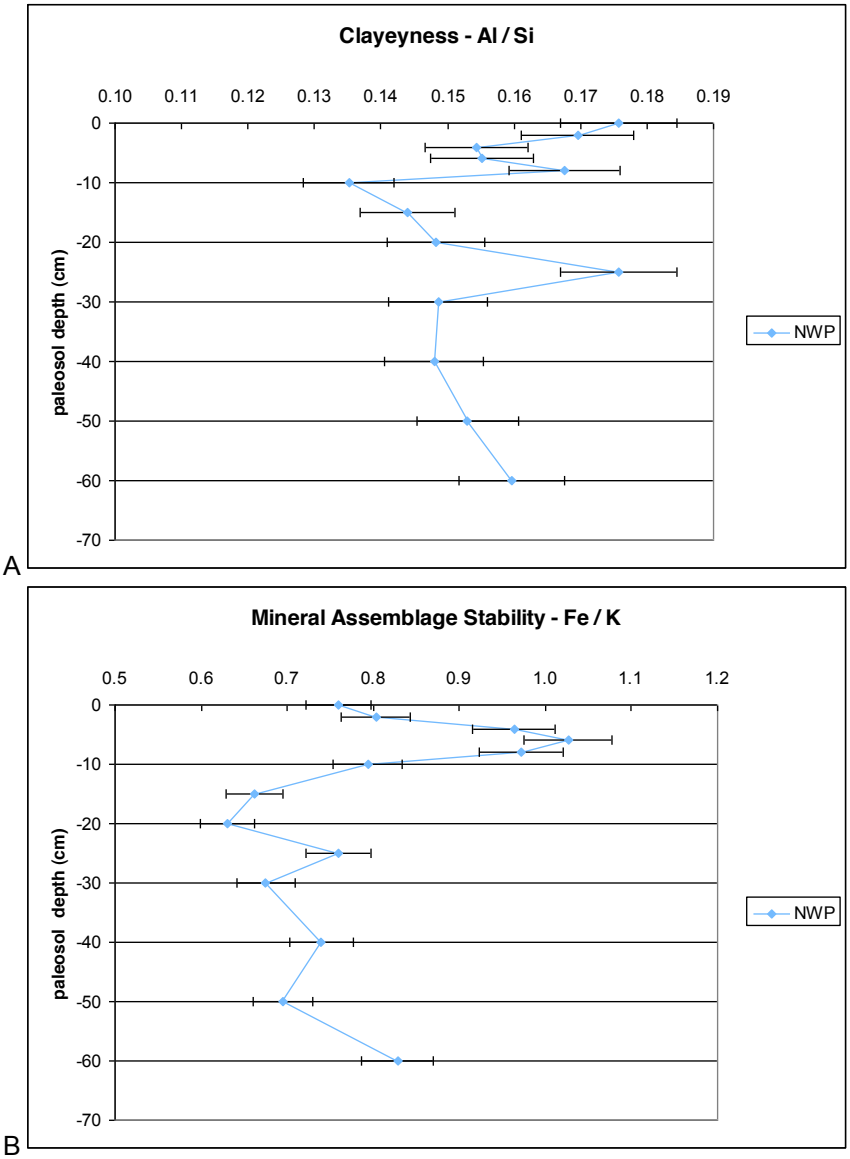

Fig. 14- Soil molecular weathering ratios plotted v. paleosol profile depth for NWP. A- Clayeyness. B- Mineral Assemblage Stability. Error bars are 5%.

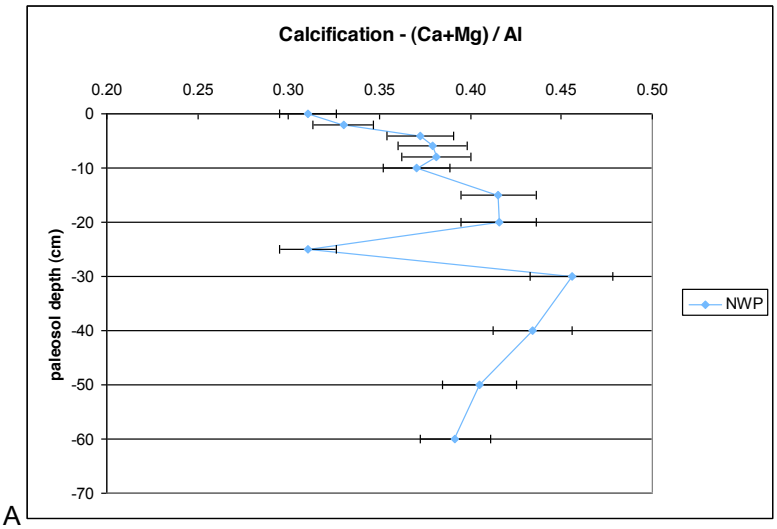

A

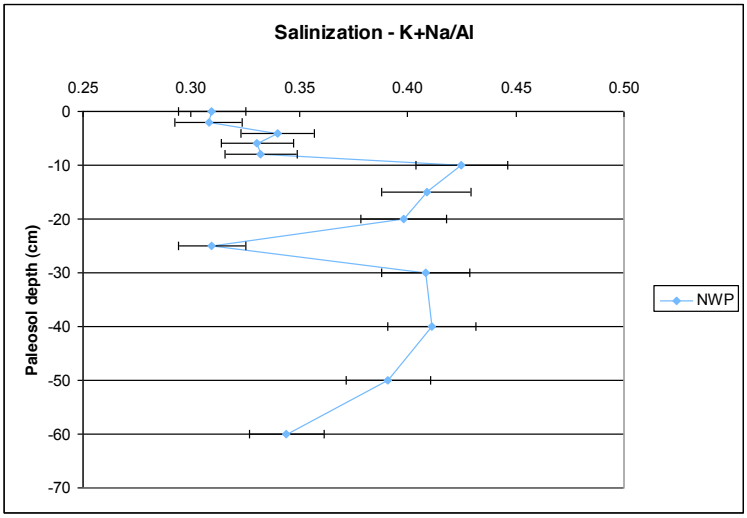

B

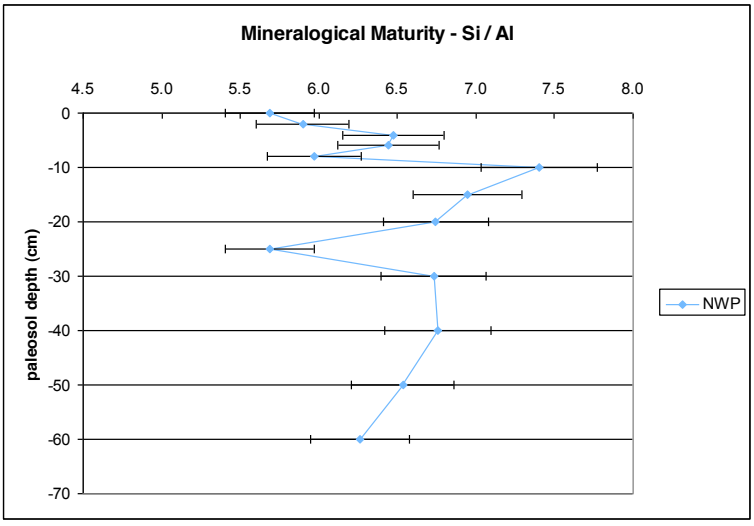

C

Fig. 15- Soil molecular weathering ratios plotted v. paleosol profile depth for NWP. A- Calcification. B- Mineralogical Maturity. C- Salinization. Error bars are 5%.

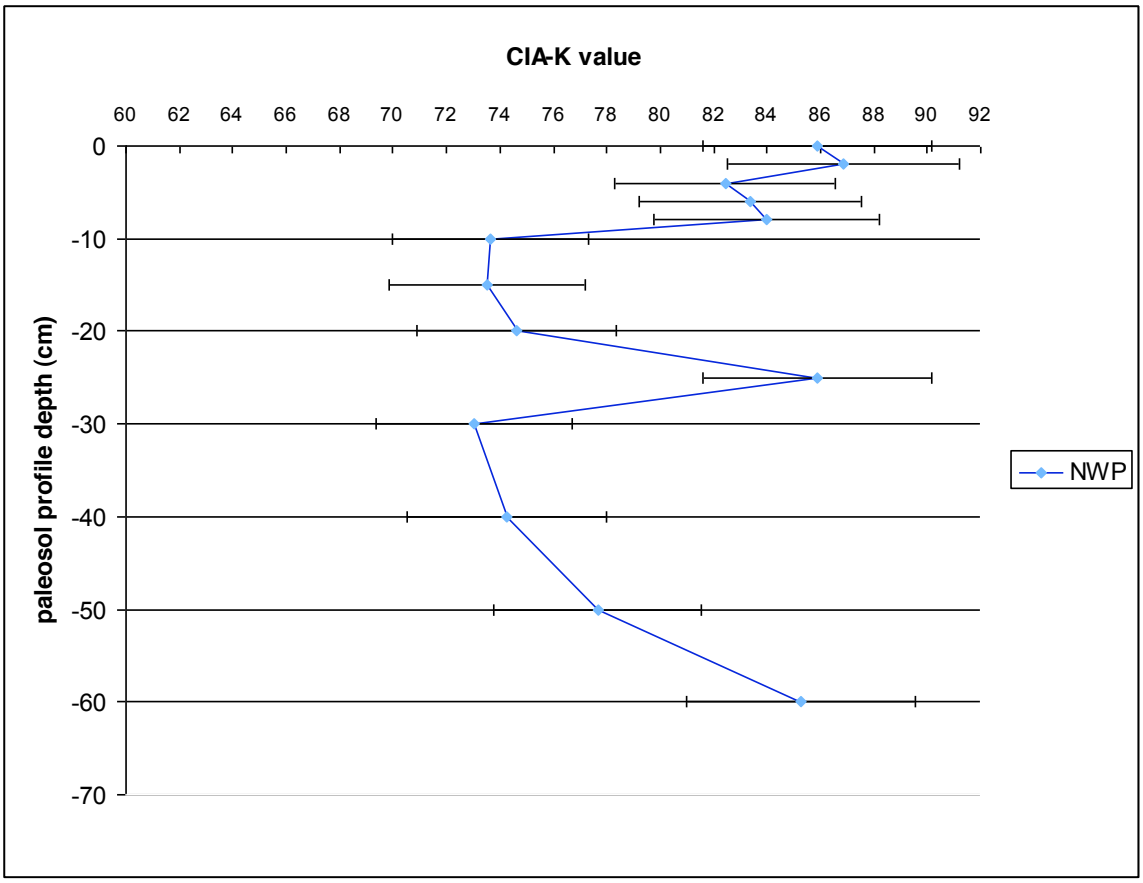

Fig. 16- CIA-K plotted v. paleosol profile depth for NWP. XRF major element data are used, and converted to molar abundances using the CIA-K conversion chart from Neil Tabor (SMU). Error bars are 5%.

Appendices

	2003 text	2003 table	Pace et al.#	Gastaldo/Rolerson *
Bada	Calcisol, high soda content, blue-gray, calcareous, high FeO/Fe2O3, gleyed soil, silty, not chemically weathered, lg calcareous nodules, deep root traces, calcareous nodules, floodplain, 8-15ka, woody root traces, *Dicynodon*	Pr, gray siltstone with shallow and scattered calcareous nodules and rhizoconcretions (Bk), semi-arid, long dry season, seasonally wet, dry bushland, *Dicynodon*, *Lystrosaurus*, floodplain depression,of silty clay, 10ka		
Barathi	Protosol, weakly developed, equisetalean roots	Tr, Bedded olive brown shale w/ fine root traces, early successional quillwort marsh, *Skolithos*, *Lystrosaurus*, lake, anabranch margin, of silty clay, 0.1ka		
Budi	Tr, gleysol, weakly developed, oligotrophic parent material, *Macanopsis* burrows, permanently waterlogged at depth, lycopsid roots	Bedded green-gray sandstone with root traces and burrows, early successional horsetail marsh, *Macanopsis*, riverside swale, q sand, 0.1ka	*Macanopsis=Katbergia*	protosol
Kerie	red/purple, drab-haloed root traces, Calcisol, not argillic, sodic, aridisol, calcareous nodules, xerosol, lg burrows, scratched/lined burrows w/ backfill, 5-8ka, woody gymnosperm roots	Tr, Reddish brown (2.5YR) with deep, well-focused calcareous nodules (Bk), subhumid seasonal, dry woodland, *Scoyenia*, *Histioderma*, *Lystrosaurus*, dry floodplain, of silty clay, 6ka	Nodules are from siltstone lithofacies, closed, wetland conditions	
Kuta	Calcisol, not argillic, sodic, aridisol, calcareous nodules, xerosol, lg burrows, 5-8ka, woody gymnosperm roots	Tr, Gray surface (A) over reddish brown (2.5YR) with shallow, well-focused calcareous nodules (Bk), subhumid moderately seasonal, dry woodland, *Histioderma*, *Lystrosaurus*, dry floodplain, of silty clay, 6ka	Nodules are from siltstone lithofacies, closed, wetland conditions	
Patha	Tr, red/purple, drab-haloed root traces, Protosol, lg burrows	Tr, reddish brown (2.5YR) with relict bedding, root traces, and burrows, riparian bushland, *Macanopsis*, *Scoyenia*, *Histioderma*, *Owenetta*, *Whaitsiid*, *Proterosuchus*, *Lystrosaurus*, streamside levee, of silty clay, 1.5ka	Closed, wetland *Macanopsis=Katbergia*	
Pawa	Tr, Protosol, clear relict bedding, weakly developed, *Macanopsis* burrow, permanently waterlogged, gray, w/in ss paleochannels, equisetalean adventitious roots, unoxidized	Pr, bedded blue-gray shale with fine root traces, early successional horsetail marsh, *Skolithos*, *Macanopsis*, streamside clayey swale, of silty clay, 0.1ka		
Sedibo	Tr, gleysol, gray, have iron-manganese nodules, gypsum rosettes, aridisol, calcic gleysols, *Macanopsis* burrow, deep root traces, calcareous nodules, w/in ss paleochannels, 5-8ka, woody gymnosperm roots	Tr, Greenish-gray with deep, well-focused calcareous nodules (Bk), subhumid, seasonally wet, riparian woodland, *Macanopsis*, lake margin, of silty clay, 6ka		Concretions subsequent to bioturbation, calcic gleysol
Som	red/purple, drab-haloed root traces, Calcisol, comparable to Bada w/ more relict bedding, lg calcareous nodules, 2-5ka, woody root traces	Pr, gray siltstone surface (A) over purple (10R) siltstone with shallow calcareous nodules (Bk), semi-arid, long dry season, seasonally wet bushland, *Lystrosaurus*, *Moscorhinus*, dry floodplain, of silty clay, 3ka		
Zam	Protosol, clear relict bedding, lycopsid roots, oxidized	Pr, bedded purple-gray (10R) siltstone with fine root traces and burrows, early successional quillwort marsh, *Macanopsis*, *Lystrosaurus*, lake margin, of silty clay 0.1ka		

Appendix 1- Table comparing paleosol descriptions given by Retallack et al. (2003) in their classification table and in their text (Pludow, personal communication). *burrows well below water table, time gap between colonization and development of nodules, not high water table or saturated soil (not necessarily lake margin or playa lake deposits), overbank flood deposits that were incipient soils that had undergone progressive saturation, burrowing occurred in an inceptisol that was overprinted was watertable rose and altered to gleysols- calcite precipitated. Burrows characteristic of poorly developed inceptisols where water-table below living chamber, constant enviro factors prevailed in interval
#siltstone=overband deposits, bioturbation=colonization of interfluvial paleosols, seasonal but moist. Nodule horizons= formed after burrow interval became uninhabitable. Nodule horizon= increasing water table. All siltstone/nodule closed wetland. Polyphase paleosols, depth to calcic isn't original soil fabric. Inceptisols overprinted by gleysols
MY SAMPLES: green-gray with mottling/weathering to red-purple-brown, potential mm scale cross beds, potential nodule, clay chips in ss, no evidence of other burrows,

Appendix 2 – ICP-OES acid digestion procedure (Scheck; Crapster-Pregont, personal communication).

1. Place several grams of sample in platinum crucibles, and ash in a muffle furnace at 550˚C for 3 hours.
2. Weigh out powdered sample (~25 mg) into labeled Teflon vial
3. Add 15 drops concentrated trace-metal-grade HNO3 and 66 drops concentrated HF. Cap and set on hotplate at ~100°C (thermostat) overnight (longer periods necessary for some samples).
4. Uncap and dry down.
5. Break up solid with 15 drops HNO3. Swirl and sonicate as necessary.
6. Dry down.
7. Add 18 drops HNO3 and 48 drops concentrated trace-metal-grade HCl. Cap and place on hotplate at ~100°C (thermostat) overnight.
8. Swirl vials, hold on side up to the light, and rotate to check for solids. Be careful not to get any samples in the cap or ribbing.

If no solids are present proceed to step 9a.
If white solids are present proceed to step 9b.

9a. Dry down half way and add 10 drops HCl. Check for solids.
If no solids are present proceed to step 10. (Small dark solids are acceptable)
If there are white solids present proceed to step 9b.

9b. Sonicate and check for solids.
If no solids are present go to step 9a.
If solids are present add more HCl, sonicate and/or reflux, then go to step 7.

10. Dry down until glossy.
11. Add 6 drops trace-metal-grade 3% HNO3, swirl, heat slightly then add 4 more drops 3% HNO3.
12. Hold up to the light and check for solids.

If no solids are present proceed to step 13a.
If solids are present let sit overnight. Check for solids.
When solids are absent proceed to step 13a.
When solids are present proceed to step 13b.

13a. Transfer to acid washed 15mL falcon tube.
13b. Sonicate and/or dry down then add 10 drops HNO3, swirl and go to step 10. (Alternative: 5 drops HNO3 and 15 drops HCl then go back to step 9a.)

14. Rinse the Teflon vial with 15 drops 3% HNO3 rolling the vial carefully to capture the entire sample. Transfer to corresponding falcon tube.
15. Rinse the Teflon vial with 8 drops 3% HNO3. Transfer to corresponding falcon tube.
16. Cap the falcon tube and place in test-tube rack.
17. Dilute and extract needed volumes for dilutions.

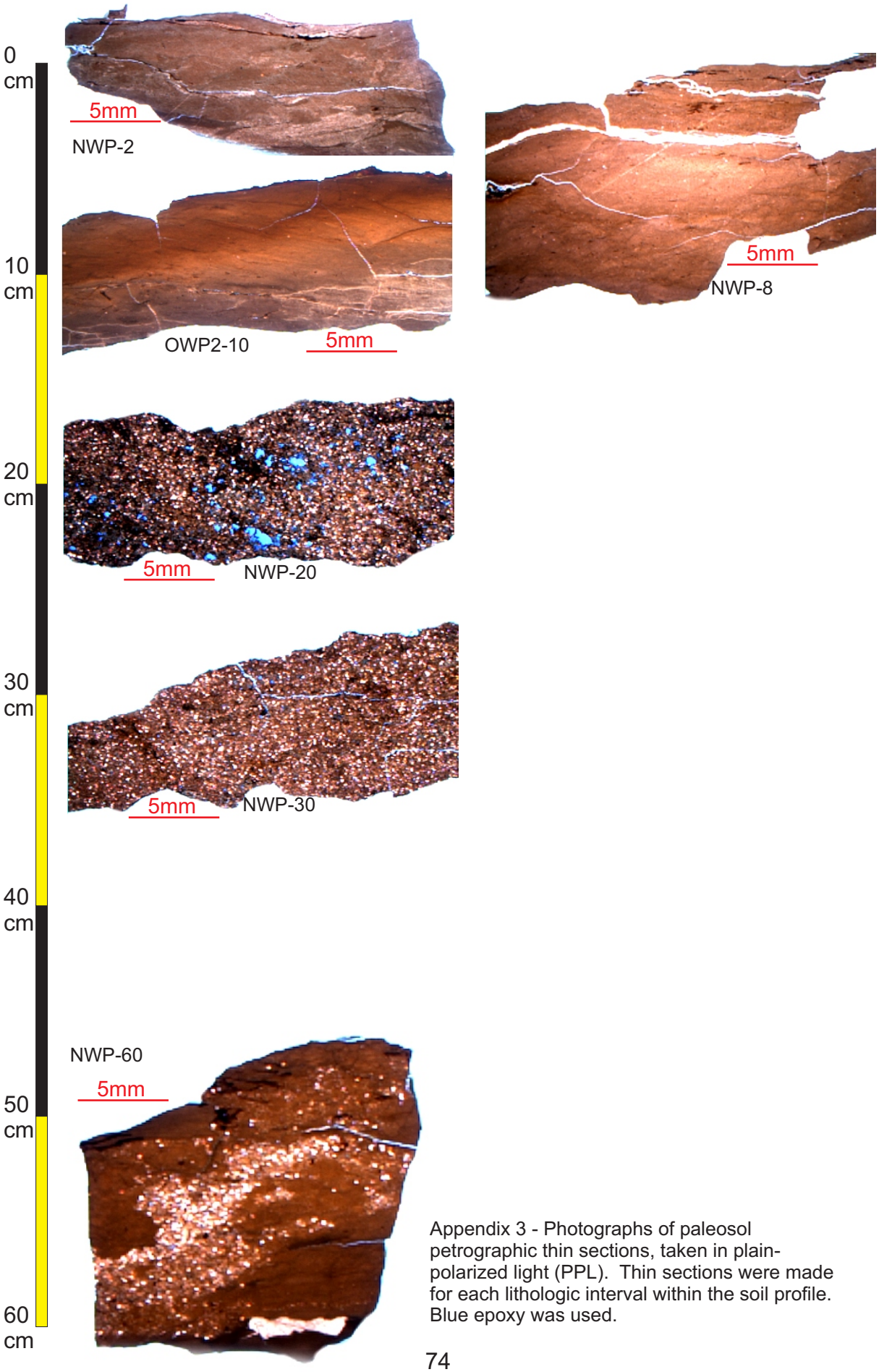

Appendix 3 - Photographs of paleosol petrographic thin sections, taken in plain-polarized light (PPL). Thin sections were made for each lithologic interval within the soil profile. Blue epoxy was used.

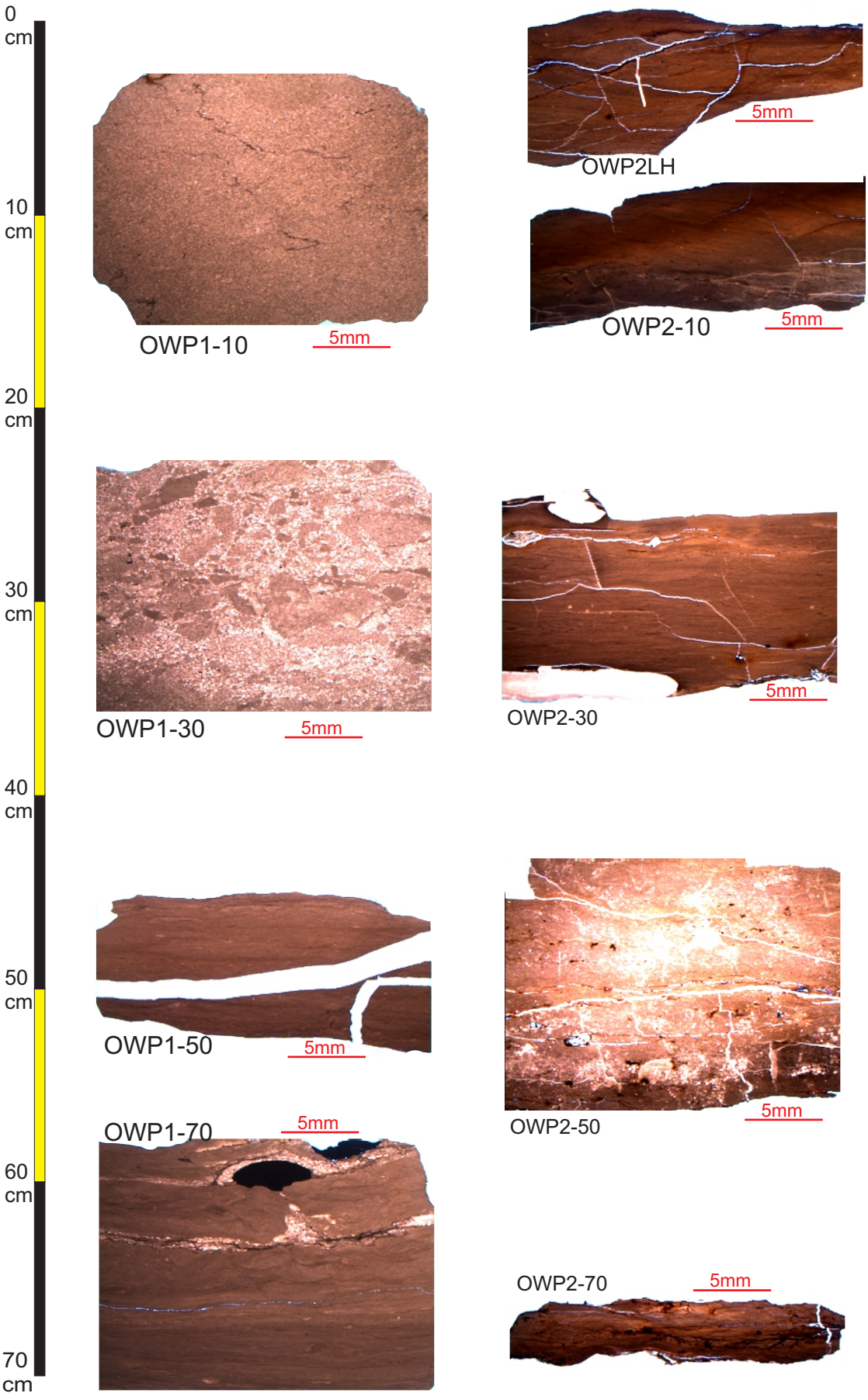

Appendix 3 continued.

Appendix 4 – XRD Spectra for analyzed clay slides for NWP. A.- NWP-10. B.- NWP-60.

A.

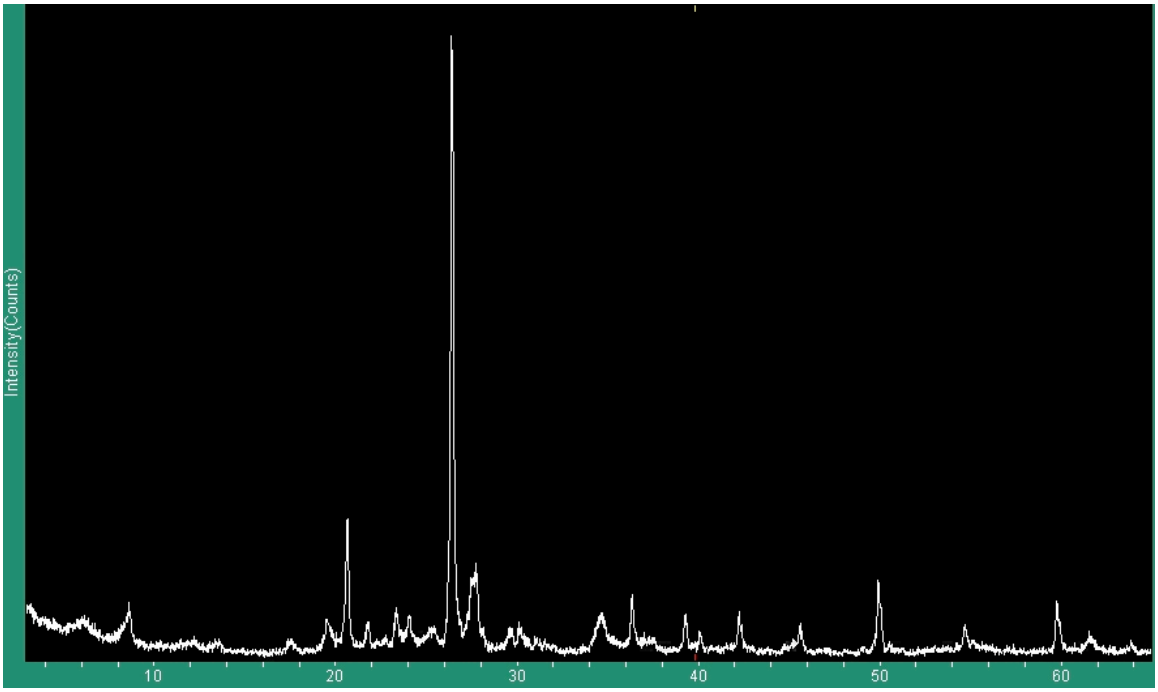

B.